AD-A038 092 MISSISSIPPI STATE UNIV MISSISSIPPI STATE ENGINEERING--ETC F/G 20/4
NUMERICAL SOLUTION OF THE NAVIER-STOKES EQUATIONS FOR 2D HYDROF--ETC(U)
FEB 77 J F THOMPSON, S P SHANKS, R L WALKER N00014-74-C-0373
UNCLASSIFIED MMSU-EIRS-ASE-77-5 NL

| OF |
ADA038092

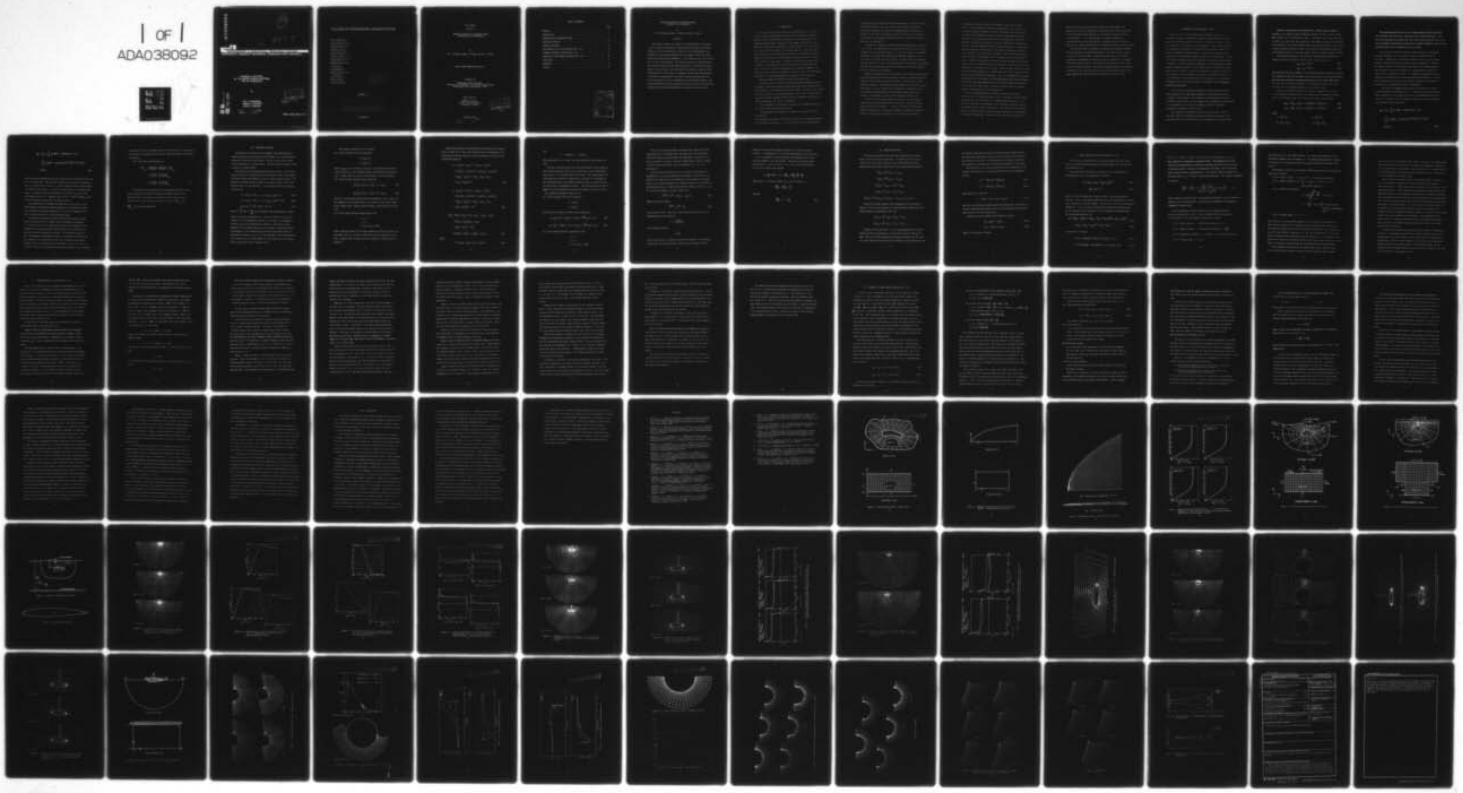

END

DATE
FILMED
4-77

EIRS
ENGINEERING & INDUSTRIAL RESEARCH STATION
AEROPHYSICS & AEROSPACE ENGINEERING / MISSISSIPPI STATE UNIVERSITY

NUMERICAL SOLUTION OF THE NAVIER-STOKES EQUATIONS FOR 2D HYDROFOILS

by

JOE F. THOMPSON,
SAMUEL P. SHANKS
& RAY L. WALKER

MSSU-EIRS-ASE-77-5

COLLEGE OF ENGINEERING ADMINISTRATION

HARRY C. SIMRALL, M.S.
DEAN, COLLEGE OF ENGINEERING

WILLIE L. MCDANIEL, JR., PH.D.
ASSOCIATE DEAN

WALTER R. CARNES, PH.D.
ASSOCIATE DEAN

LAWRENCE J. HILL, M.S.
DIRECTOR, ENGINEERING EXTENSION

CHARLES B. CLIETT, M.S.
AEROPHYSICS & AEROSPACE ENGINEERING

WILLIAM R. FOX, PH.D.
AGRICULTURAL & BIOLOGICAL ENGINEERING

JOHN L. WEEKS, JR., PH.D.
CHEMICAL ENGINEERING

ROBERT M. SCHOLTES, PH.D.
CIVIL ENGINEERING

B. J. BALL, PH.D.
ELECTRICAL ENGINEERING

W. H. EUBANKS, M.ED.
ENGINEERING GRAPHICS

FRANK E. COTTON, JR., PH.D.
INDUSTRIAL ENGINEERING

C. T. CARLEY, PH.D.
MECHANICAL ENGINEERING

JOHN I. PAULK, PH.D.
NUCLEAR ENGINEERING

ELDRED W. HOUGH, PH.D.
PETROLEUM ENGINEERING

For additional copies or information
address correspondence to:

ENGINEERING AND INDUSTRIAL RESEARCH STATION
DRAWER DE
MISSISSIPPI STATE UNIVERSITY
MISSISSIPPI STATE, MISSISSIPPI 39762

TELEPHONE (601) 325-2266

Final Report

entitled

NUMERICAL SOLUTION OF THE NAVIER-STOKES EQUATIONS FOR 2D HYDROFOILS

By

Joe F. Thompson, Samuel P. Shanks, and Ray L. Walker

Report Number MMSU-EIRS-ASE-77-5

Prepared by

Mississippi State University
Department of Aerophysics and Aerospace Engineering
Mississippi State, Mississippi 39762

Under Contract

N00014-74-C-0373
Office of Naval Research
Arlington, Virginia

February 1977

TABLE OF CONTENTS

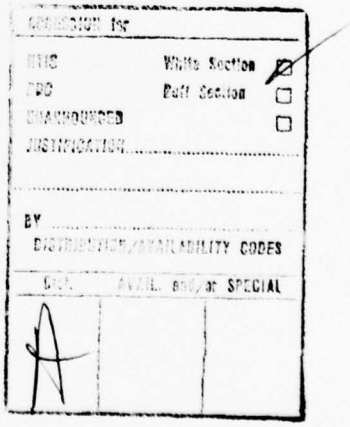

NUMERICAL SOLUTION OF THE NAVIER-STOKES EQUATIONS FOR 2D HYDROFOILS

by

Joe F. Thompson, Samuel P. Shanks, and Ray L. Walker

Abstract

This report presents the results of an investigation of the application of numerically-generated boundary-fitted curvilinear coordinate systems in the finite-difference solution of the time-dependent, two-dimensional Navier-Stokes equations for the laminar viscous flow about hydrofoils moving either submerged at a finite depth or in a free surface of a fluid of infinite depth. The hydrofoil may be of arbitrary shape, and its motion may include pitching oscillation or oscillation normal or parallel to the plane of the undisturbed free surface as well as translation parallel to this plane. A computer code has been developed that is capable of predicting the flow field, pressure distributions, and force coefficients for this configuration at low Reynolds numbers. The finite-difference solution is implicit in time so that all the difference equations are solved simultaneously by iteration at each time step.

I. INTRODUCTION

This report presents the results of an investigation of the application of numerically-generated boundary-fitted curvilinear coordinate systems in the finite-difference solution of the time-dependent, two-dimensional Navier-Stokes equations for the laminar viscous flow about hydrofoils moving either submerged at a finite depth or in a free surface of a fluid of infinite depth. The hydrofoil may be of arbitrary shape, and its motion may include pitching oscillation or oscillation normal or parallel to the plane of the undisturbed free surface as well as translation parallel to this plane. A computer code has been developed that is capable of predicting the flow field, pressure distributions, and force coefficients for this configuration at low Reynolds numbers. The finite-difference solution is implicit in time so that all the difference equations are solved simultaneously by iteration at each time step.

This investigation consisted essentially of three parts:

(1) Verification of the use of numerically-generated boundary-fitted curvilinear coordinate systems in Navier-Stokes solutions by application of the technique to the unbounded high Reynolds number flow past a semi-infinite flat plate parallel to the undisturbed flow. The results from this solution gave excellent comparison with the Blasius boundary layer solution in the region where the latter is applicable.

(2) Development of the numerical solution for a submerged hydrofoil at a finite depth below the free surface.

(3) Development of the numerical solution for a hydrofoil in the free surface.

The procedures and results of these three solutions are summarized herein. The *concomitant* References 1, 2, and 3, produced by this investigation,

contain the details and more extensive presentations of results from the above-mentioned Parts (1), (2), and (3) of the study, respectively. These three documents are available from Mississippi State University. Results for the finite flat plate of Part (1) have also been reported in References 4 and 5, while preliminary results from Parts (2) and (3) were given in Reference 6.

The numerical solution of the Navier-Stokes equations for flow with a free surface is complicated in particular by the fact that part of the boundary of the calculation region, i.e., the free surface, is deforming. This makes the accurate representation of boundary conditions on the free surface difficult; yet this solution, as other partial differential equation solutions, is most strongly influenced by the boundary conditions. The most critical need for accuracy thus lies in precisely the region of the most difficulty of attainment.

Numerical solutions for this free surface flow problem have generally tracked the moving free surface through a fixed grid, using interpolation among the fixed regularly spaced grid points to represent the surface boundary conditions. Similarly, solid body shapes in the flow have either been simple, so as to coincide with rectangular or cylindrical grids, or have been represented also by interpolation among grid points. A survey of such methods is given in the concomitant Reference (2).

The basis of the present numerical solution is the technique of numerically-generated boundary-fitted curvilinear coordinate systems reported earlier in Reference 7. This is a procedure for automatic numerical generation of curvilinear coordinate systems with coordinate lines coincident with all boundaries of a general multi-connected,

two-dimensional region containing any number of arbitrarily shaped bodies. The curvilinear coordinates are generated as the solution of an elliptic partial differential system. No restrictions are placed on the shape of the boundaries, which may even be time-dependent, and the approach is not restricted in principle to two dimensions. With this procedure the numerical solution of a partial differential system may be done on a fixed rectangular field with a square mesh with no interpolation required regardless of the shape of the physical boundaries, regardless of the spacing of the curvilinear coordinate lines in the physical field, and regardless of the movement of the coordinate system in the physical plane. A number of examples of coordinate systems and application thereof to the solution of partial differential equations is given in [8] and [9], along with a discussion of the technique. This procedure essentially eliminates the boundary geometry as a complicating factor in the numerical solution of partial differential equations. The use of boundary-fitted coordinate systems for the solution of the incompressible Navier-Stokes equations for the flow about two-dimensional airfoils has been reported by Thames, et. al. [4] and by Hodge [10]. The latter reference uses the pressure-velocity formulation used in the present work.

The use of boundary-fitted coordinate systems is particularly attractive for free surface problems, since a coordinate line will remain coincident with the free surface as it deforms under wave action. The physical flow field is transformed to the curvilinear coordinate system as discussed in more detail in Section II. The field in the transformed plane is rectangular with a fixed square grid regardless of the movement of the physical boundaries. With the partial differential equations of

motion and their associated boundary conditions transformed to the curvilinear system, all computation can be done on the fixed square grid in the transformed plane regardless of the motion of the free surface or the hydrofoil. It is even possible to allow the hydrofoil to oscillate without really complicating the problem, since a coordinate line can also remain coincident with the hydrofoil surface as it oscillates.

The present solution is capable of treating the low Reynolds number viscous flow about a translating hydrofoil in or below the free surface of a fluid of infinite depth. The hydrofoil may also be in pitching, plunging, or longitudinal oscillation as well as translation. The hydrofoil starts from rest with a flat surface and accelerates to full speed at any acceleration desired. The general solution procedure is discussed in Sections II-IV, and facets peculiar to each of the three parts of the study together with typical results are given in Sections V-VIII.

II. BOUNDARY-FITTED COORDINATE SYSTEM

The basic idea of the boundary-fitted coordinate systems is to numerically generate a curvilinear coordinate system having some coordinate line coincident with each boundary of the physical region of interest, regardless of the shape of these boundaries. This is done by taking the curvilinear coordinates to be solutions of an elliptic partial differential system, with constant values of one of the curvilinear coordinates specified as Dirichlet boundary conditions on each boundary. Values of the other coordinate are either specified in a monotonic variation over a boundary as Dirichlet boundary conditions, or are determined by Neumann boundary conditions thereon. In the latter case, the curvilinear coordinate lines can be made to intersect the boundary according to some specified condition, such as normalcy or parallel to some given direction. It is also possible to exercise control over the spacing of the curvilinear coordinate lines in the field in order to concentrate lines in regions of expected high gradients.

In any case, the numerical generation of the coordinate system is done automatically for any shape boundaries, requiring only the input of points on the boundary. The technique has been described in detail in earlier reports [7-9], and the computer code, together with instructions for and examples of its use in the numerical solution of partial differential equations, is given in [9].

The technique is described in general in this section. Each of the three parts of the present study used a different variation of the basic procedure as is discussed for each configuration in Sections V-VII.

Consider transforming the two-dimensional, doubly-connected region D, bounded by two, simple, closed, arbitrary contours, Γ_1 and Γ_2, onto a rectangular region, D*, as illustrated in Fig. 1. We require that Γ_1 map onto Γ_1*, Γ_2 onto Γ_2*, Γ_3 onto Γ_3*, and Γ_4 onto Γ_4*. Note that Γ_1* and Γ_2* are required to be constant η-lines, while the arbitrary cut between contours Γ_1 and Γ_2 (i.e., Γ_3 and Γ_4) becomes constant ξ-lines. The region D is the physical plane, D* the transformed plane, Γ_1 the body contour, and Γ_2 the remote boundary contour.

As discussed previously, the curvilinear coordinates are generated by solving an elliptic system of suitable form. One such system is

$$\xi_{xx} + \xi_{yy} = P(\xi,\eta) \tag{1a}$$

$$\eta_{xx} + \eta_{yy} = Q(\xi,\eta) \tag{1b}$$

with Dirichlet boundary conditions, one coordinate being specified to be equal to a constant on the body and equal to another constant on the outer boundary, with the other coordinate varying monotonically over the same range around both the body and the outer boundary. This system was used for the finite flat plate and the submerged hydrofoil in the present study.

Since it is desired to perform all numerical computations in the uniform rectangular transformed plane, the dependent and independent variables must be interchanged in Eq. (1). This results in the coupled system

$$\alpha x_{\xi\xi} - 2\beta x_{\xi\eta} + \gamma x_{\eta\eta} = -J^2[x_\xi P(\xi,\eta) + x_\eta Q(\xi,\eta)] \tag{2a}$$

$$\alpha y_{\xi\xi} - 2\beta y_{\xi\eta} + \gamma y_{\eta\eta} = -J^2[y_\xi P(\xi,\eta) + y_\eta Q(\xi,\eta)] \tag{2b}$$

where

$$\alpha = x_\eta^2 + y_\eta^2 \qquad \gamma = x_\xi^2 + y_\xi^2$$

$$\beta = x_\xi x_\eta + y_\xi y_\eta \qquad J = x_\xi y_\eta - x_\eta y_\xi$$

The system described by Eq. (2) is a quasi-linear elliptic system for the coordinate functions $x(\xi,\eta)$ and $y(\xi,\eta)$ in the transformed plane. This set is considerably more complex than the linear system specified by Eq. (1), but the boundary conditions are specified on straight bonndaries, and the coordinate spacing in the transformed plane is uniform.

The ξ=constant lines may be spaced as desired around the boundaries, since the assignment of the ξ-values to the [x,y] boundary points is arbitrary. (Numerically, the discrete boundary values $[x_k,y_k]$ are transformed to equi-spaced discrete ξ_k-points on both boundaries.) Control of the radial spacing of the η=constant lines and of the incidence angle of the ξ=constant lines at the boundaries is accomplished by varying the functions $P(\xi,\eta)$ and $Q(\xi,\eta)$ in (2). All numerical computations, both to generate the boundary-fitted coordinate system and subsequently to utilize the coordinates for solving a set of partial differential equations, are executed on a rectangular field with a uniform grid.

The effect of changing the functions $P(\xi,\eta)$ and $Q(\xi,\eta)$ on the coordinate system is discussed in Ref. 9. One particularly effective procedure, used here for the finite flat plate and submerged hydrofoil solutions, is to choose P and Q as exponential terms, so that the coordinates are generated as the solutions of

$$\xi_{xx} + \xi_{yy} = -\sum_{i=1}^{n} a_i \, \mathrm{sgn}(\xi - \xi_i)\exp(-c_i|\xi - \xi_i|)$$

$$- \sum_{j=1}^{m} b_j \, \mathrm{sgn}(\xi - \xi_j)\exp(-d_j\sqrt{(\xi - \xi_j)^2 + (\eta - \eta_j)^2})$$

$$\equiv P(\xi,\eta) \qquad (3a)$$

$$\eta_{xx} + \eta_{yy} = -\sum_{i=1}^{n} a_i \, \mathrm{sgn}(\eta - \eta_i)\exp(-c_i|\eta - \eta_i|)$$

$$- \sum_{j=1}^{m} b_j \, \mathrm{sgn}(\eta - \eta_j)\exp(-d_j\sqrt{(\xi - \xi_j)^2 + (\eta - \eta_j)^2})$$

$$\equiv Q(\xi,\eta) \qquad (3b)$$

where the positive amplitudes and decay factors are not necessarily the same in the two equations. Here the first terms have the effect of attracting the ξ = constant lines to the $\xi = \xi_i$ lines in Equation (3a), and attracting η = constant lines to the $\eta = \eta_i$ lines in Equation (3b). The second terms cause ξ = constant lines to be attracted to the points (ξ_j,η_j) in (3a), with similar effect on η = constant lines in (3b). Several examples of the use of coordinate system control are given in Ref. 9.

The transformation technique developed above can be used to solve time-dependent problems with moving boundaries by performing all numerical calculations, without interpolation, on a fixed rectangular field with a uniform square grid in the transformed plane.

As discussed previously, the physical plane grid system is generated by solving the set of elliptic partial differential equations, (2), with one of the (ξ,η) coordinates specified to be constant on the boundaries of the physical plane, and the other (ξ,η) coordinate distributed along the boundaries as desired. If the boundary values of x and y are changed in the physical plane by the movement of the free surface contours a new solution of the elliptic system with the changed boundary values is obtained over the same range of values of ξ and η in the field. Thus, the transformed plane remains unchanged as the coordinate

grid system moves in the physical plane. Only the values of the physical coordinates (x,y) change with time at the fixed grid points in the transformed plane.

The transformed time derivative is

$$\left(\frac{\partial f}{\partial t}\right)_{x,y} = \frac{\partial(x,y,f)}{\partial(\xi,\eta,t)} \Big/ \frac{\partial(x,y,t)}{\partial(\xi,\eta,t)} = \left(\frac{\partial f}{\partial t}\right)_{\xi,\eta}$$

$$- \frac{1}{J}\left(\frac{\partial f}{\partial t}\frac{\partial y}{\partial \eta} - \frac{\partial f}{\partial \eta}\frac{\partial y}{\partial \xi}\right)\left(\frac{\partial x}{\partial t}\right)_{\xi,\eta}$$

$$+ \frac{1}{J}\left(\frac{\partial f}{\partial \xi}\frac{\partial x}{\partial \eta} - \frac{\partial f}{\partial \eta}\frac{\partial x}{\partial \xi}\right)\left(\frac{\partial y}{\partial t}\right)_{\xi,\eta} . \qquad (4)$$

All derivatives are expressed in the transformed variables (ξ,η); thus eliminating the need for interpolation between points in the physical plane. The movement of the physical plane grid points is accounted for by the time rate of change of x and y, $\left(\frac{\partial x}{\partial t}\right)_{\xi,\eta}$ and $\left(\frac{\partial y}{\partial t}\right)_{\xi,\eta}$ in the above expression.

III. EQUATIONS OF MOTION

The equations of motion are the complete time-dependent Navier-Stokes equations with the gravity term included. The no-slip boundary condition is applied on the hydrofoil, and the viscous stress conditions are applied on the free surface. The free surface deforms in time as waves are formed thereon.

All quantities are non-dimensionalized with respect to the translation velocity of the hydrofoil and the hydrofoil chord. The Reynolds and Froude numbers are defined in terms of these reference values. The physical coordinate system is taken to be fixed relative to the translational motion of the hydrofoil. In the physical plane the equations of motion are

$$u_t + (u^2)_x + (uv)_y = - p_x + (u_{xx} + u_{yy})/R - \dot{V} \tag{5a}$$

$$v_t + (uv)_x + (v^2)_y = - p_y + (v_{xx} + v_{yy})/R - 1/F^2 \tag{5b}$$

$$p_{xx} + p_{yy} = - u_x^2 - 2u_y v_x - v_y^2 - D_t \tag{5c}$$

where $R = \dfrac{V_o c}{\nu}$ and $F = \dfrac{V_o}{\sqrt{gc}}$ are the Reynolds and Froude numbers, respectively, V_o being the magnitude of a reference hydrofoil translational velocity, V the instantaneous velocity, c the chord, ν the kinematic viscosity, and g the acceleration of gravity. The third of these equations is the Poisson equation for the pressure, derived by taking the divergence of the Navier-Stokes equations and requiring that the continuity equation ($D \equiv u_x + v_y = 0$) be satisfied. The time derivative of D, ideally zero, has been retained in this equation as a corrective term in the manner of Hirt and Harlow [11].

The boundary conditions are as follows:

(a) On the hydrofoil (no-slip condition):

$$u = u_B(x,y,t)$$

$$v = v_B(x,y,t)$$

where (u_B, v_B) are the velocity components of the hydrofoil surface at (x,y,t) relative to the coordinate system translating with the hydrofoil. (These values are zero if the hydrofoil is not oscillating.)

(b) On the surface (viscous stress condition):

$$\frac{2}{R} u_x n_1 + \frac{1}{R} (u_y + v_x) n_2 = (p - p_o) n_1 \qquad (6a)$$

$$\frac{2}{R} v_y n_2 + \frac{1}{R} (u_y + v_x) n_1 = (p - p_o) n_2 \qquad (6b)$$

where p_o is the applied pressure from the atmosphere, and n_1 and n_2 are the components of the unit normal to the surface in the x and y directions, respectively. These relations assume no wind stress on the surface.

(c) On the remote boundary (undisturbed flow):

$$u = - V$$

$$v = 0$$

$$p = p_o + (y_o - y)/F^2$$

(These conditions apply on the remote boundary strictly only until surface waves reach it. At low R, sufficient viscous dissipation is present to damp the waves before the remote boundary 10 chords distant is reached.)

Using the derivative transformation relations given in the appendices of either [2] or [9], these equations may be transformed to the curvilinear coordinate system, so that the equations of motion in the transformed plane are

$$u_t - x_t(y_\eta u_\xi - y_\xi u_\eta)/J - y_t(x_\xi u_\eta - x_\eta u_\xi)/J$$

$$+ [y_\eta (u^2)_\xi - y_\xi (u^2)_\eta]/J + [x_\xi (uv)_\eta - x_\eta (uv)_\xi]/J$$

$$+ (y_\eta p_\xi - y_\xi p_\eta)/J = (\alpha u_{\xi\xi} - 2\beta u_{\xi\eta} + \gamma u_{\eta\eta}$$

$$+ \sigma u_\eta + \tau u_\xi)/RJ^2 + \dot{V} \qquad (7a)$$

$$v_t - x_t(y_\eta v_\xi - y_\xi v_\eta)/J - y_t(x_\xi v_\eta - x_\eta v_\xi)/J$$

$$+ [y_\eta (uv)_\xi - y_\xi (uv)_\eta]/J + [x_\xi (v^2)_\eta - x_\eta (v^2)_\xi]/J$$

$$+ (x_\xi p_\eta - x_\eta p_\xi)/J = (\alpha v_{\xi\xi} - 2\beta v_{\xi\eta} + \gamma v_{\eta\eta}$$

$$+ \sigma v_\eta + \tau v_\xi)/RJ^2 - 1/F^2 \qquad (7b)$$

$$\alpha p_{\xi\xi} - 2\beta p_{\xi\eta} + \gamma p_{\eta\eta} + \sigma p_\eta + \tau p_\xi = -(y_\eta u_\xi - y_\xi u_\eta)^2$$

$$- 2(x_\xi u_\eta - x_\eta u_\xi)(y_\eta v_\xi - y_\xi v_\eta)$$

$$- (x_\xi v_\eta - x_\eta v_\xi)^2 - J^2 D_t$$

$$+ x_t(D_\xi y_\eta - D_\eta y_\xi)J - y_t(D_\xi x_\eta - D_\eta x_\xi)J \qquad (7c)$$

where

$$D = (y_\eta u_\xi - y_\xi u_\eta + x_\xi v_\eta - x_\eta v_\xi)/J \qquad (7d)$$

and

$$\sigma \equiv J^2 Q(\xi,\eta) \ , \ \tau \equiv J^2 P(\xi,\eta) \ .$$

The coefficients α, β, γ, and J have been defined in the previous section.

The time derivatives have also been transformed in these equations. Thus, time derivatives in Eq. (7) are taken with ξ and η fixed, while those in Eq. (5) were taken with x and y fixed. This transformation of time derivatives allows the computation to be done on a fixed grid in the transformed plane even though the physical grid is in motion due to the free surface and hydrofoil movement. The same procedure was used by Shanks [2] and is discussed in more detail therein, as well as in [9].

The transformed boundary conditions are

(a) On the hydrofoil (no-slip conditions):

$$u = u_B(\xi,t)$$

$$v = v_B(\xi,t)$$

(b) on the free surface (viscous stress conditions):

$$u_\xi = \frac{1}{\alpha^2}\left[(\alpha\beta - Jx_\eta y_\eta)u_\eta + (Jx_\eta^2)v_\eta + \frac{RJ\alpha}{2}\, y_\eta(p - p_o)\right] \qquad (8a)$$

$$v_\xi = \frac{1}{\alpha^2}\left[(-\, Jy_\eta^2)u_\eta + (\alpha\beta + Jx_\eta y_\eta)v_\eta - \frac{RJ\alpha}{2}\, x_\eta(p - p_o)\right] \qquad (8b)$$

(c) On the remote boundary (undisturbed flow):

$$u = -\, V$$

$$v = 0$$

$$p = p_o + (y_o - y)/F^2$$

The two free surface boundary conditions given above result from transforming the two viscous stress equations (6) to the curvilinear coordinate system and solving these two simultaneous equations for u_ξ and v_ξ in terms of u_η and v_η, the free surface being a line of constant ξ in the configuration used. (See the appendix of [2] for this development.)

On the hydrofoil contour and the free surface, the pressure is determined by iteratively adjusting the pressure at each point on the hydrofoil in proportion to the divergence of the velocity at the same point, so that upon convergence the continuity equation is satisfied at the hydrofoil surface. Thus on the hydrofoil surface, since $u_\xi = v_\xi = 0$ by the no-slip condition, we have, using (7d),

$$p^{(k+1)} = p^{(k)} - K(x_\xi v_\eta - y_\xi u_\eta)/J \tag{9a}$$

while on the free surface,

$$p^{(k+1)} = p^{(k)} - KD \tag{9b}$$

with D given by (7d). Here (k) is the iteration counter, and K is a proportionality factor given by

$$K = \frac{2\omega J^2}{(\alpha + \gamma)\Delta t}$$

on the hydrofoil and by

$$K = \frac{1}{R}$$

on the free surface, ω being an acceleration parameter. The different form on the free surface results from the need to prevent positive

feedback from the surface stress condition to the surface pressure iteration. See Appendix D of [3] for the development of these relations.

The y coordinate on the free surface is determined at each time from the movement of the free surface. Since the free surface can be described by $y = f(x,t)$ or $f(x,t) - y = 0$, the convective derivative of the latter function must vanish:

$$0 = \frac{d}{dt}\,[f(x,t) - y] = \left(\frac{\partial f}{\partial t}\right)_x + \left(\frac{\partial f}{\partial x}\right)_t \frac{dx}{dt} - \frac{dy}{dt}$$

Then since $y = f$, and the surface is a line of constant ξ,

$$\left(\frac{\partial y}{\partial x}\right)_t = \left(\frac{\partial y}{\partial x}\right)_\xi = \frac{y_\eta}{x_\eta}$$

and then

$$\left(\frac{\partial y}{\partial t}\right)_x = v - u\,\frac{y_\eta}{x_\eta} \tag{10}$$

IV. NUMERICAL SOLUTION

All space derivatives in the field are approximated by second-order, central difference expressions. ($\Delta\xi$ and $\Delta\eta$ are both unity by construction, the actual values of ξ and η being immaterial since cancellation occurs after substitution in the transformed equations.):

$$(f_\xi)_{ij} \cong \frac{1}{2}\,(f_{i+1,j} - f_{i-1,j})$$

$$(f_\eta)_{ij} \cong \frac{1}{2}\,(f_{i,j+1} - f_{i,j-1})$$

$$(f_{\xi\xi})_{ij} \cong f_{i+1,j} - 2f_{ij} + f_{i-1,j}$$

$$(f_{\eta\eta})_{ij} \cong f_{i,j+1} - 2f_{ij} + f_{i,j-1}$$

$$(f_{\xi\eta})_{ij} \cong \frac{1}{4}\,(f_{i+1,j+1} - f_{i+1,j-1} - f_{i-1,j+1} + f_{i-1,j-1})$$

Derivatives along coordinate lines emanating from the hydrofoil surface or from the free surface are evaluated using second-order, one-sided difference expressions of the form

$$(f_\xi)_{1,j} = \frac{1}{2}\,(-f_{3,j} + 4f_{2,j} - 3f_{1,j})$$

$$(f_\eta)_{i,1} = \frac{1}{2}\,(-f_{i,3} + 4f_{i,2} - 3f_{i,1})$$

Finally all the time derivatives are approximated by first-order, backward difference expressions, so that the solution is implicit in time. The set of five simultaneous difference equations from (2) and (7), three equations of motion and two coordinate system equations, with

the boundary conditions are solved at each time step by SOR iteration. The result from the previous time step serves as the initial guess for the iteration at the next. The solution starts from rest with a flat free surface and proceeds with a specified acceleration to full speed.

The body force components are obtained from the integration of the pressure and shear forces around the wetted portion of the hydrofoil surface:

$$F_x = -2 \oint p y_\xi d\xi + \frac{2}{R} \oint \omega x_\xi d\xi \tag{11a}$$

$$F_y = +2 \oint p x_\xi d\xi + \frac{2}{R} \oint \omega y_\xi d\xi \tag{11b}$$

with vorticity, ω, given by

$$\omega = (y_\eta v_\xi - y_\xi v_\eta - x_\xi u_\eta + x_\eta u_\xi)/J \tag{12}$$

Here the η-derivatives are evaluated by the second-order, one-sided difference expressions given above, while the second-order central expressions are used for the ξ-derivatives.

Finally, the lift and drag coefficients are given by

$$C_L = F_y \cos\theta - F_x \sin\theta \tag{13a}$$

$$C_D = F_y \sin\theta + F_x \cos\theta \tag{13b}$$

where θ is the angle of attack.

V. SEMI-INFINITE FLAT PLATE SOLUTION (Ref. [1])

This solution was developed in the stream function-vorticity formulation of the Navier-Stokes equations following Thames [12], and has also been reported in [5].

The stream function-vorticity formulation of the two-dimensional, incompressible viscous flow equations is given by

$$\omega_t + \psi_y\omega_x - \psi_x\omega_y = (\omega_{xx} + \omega_{yy})/R \tag{14a}$$

$$\psi_{xx} + \psi_{yy} = -\omega \tag{14b}$$

where ψ is the non-dimensional stream function, ω the non-dimensional vorticity, and R is the Reynolds number based on the characteristic velocity (free stream value) and body length. The set (14) is in the non-conservative formulation. Eqs. (14) may be transformed utilizing the operations given in [9] yielding the set applicable in the rectangular transformed plane. The transformed equations are:

$$\omega_t + (\psi_\eta\omega_\xi - \psi_\xi\omega_\eta)/J = (\alpha\omega_{\xi\xi} - 2\beta\omega_{\xi\eta} + \gamma\omega_{\eta\eta})/J^2R + (Q\omega_\eta + P\omega_\xi)/R \tag{15a}$$

$$(\alpha\psi_{\xi\xi} - 2\beta\psi_{\xi\eta} + \gamma\psi_{\eta\eta})/J^2 + Q\psi_\eta + P\psi_\xi = -\omega \tag{15b}$$

with boundary conditions

$$\psi = \psi_o = \text{constant},\ \sqrt{\gamma}\,\psi_\eta/J = 0,\ [\xi,\eta_1] \in \Gamma_1^* \tag{15c}$$

$$\psi = y(\xi,\eta_2)\cos\Theta - x(\xi,\eta_2)\sin\Theta,\ \omega = 0,\ [\xi,\eta_2] \in \Gamma_2^* \tag{15d}$$

where θ is the angle of attack. The second of (15c) guarantees that the no-slip condition is satisfied on the body surface. The satisfaction of this condition is accomplished by iteratively adjusting the value of the vorticity on the body surface, utilizing a false-position procedure, until the second-order forward difference approximation to the velocity component tangential to the body surface, $V_{\tau} = \sqrt{\gamma}\,\psi_{\eta}/J$, is below some tolerance. The iterative algorithm is given by

$$\omega_{i,1}^{(k+1)} = \omega_{i,1}^{(k)} - \delta \frac{\omega_{i,1}^{(k)} - \omega_{i,1}^{(k-1)}}{(V_{\tau_\eta})_{i,1}^{(k)} - (V_{\tau_\eta})_{i,1}^{(k-1)}} (V_{\tau_\eta})_{i,1}^{(k)} \qquad (16)$$

where k denotes iteration count, δ an adjustable parameter, and (i,1) refers to some point on the body surface. This method is an extension of an approach suggested by Israeli [13].

The transformation from the physical to the transformed field is indicated schematically in Fig. 2. The coordinate system was generated as the solution of (2) with boundary conditions as follows:

on a'b' (plate surface): x = specified as desired, y = 0.

on a'c' (upper boundary): x = specified as desired, $y = 10(\frac{x}{R})^{\frac{1}{2}}$.

on b'c' (downstream boundary): x = constant, y = specified as desired.

on a'a' (leading edge): x = y = 0.

The condition on y on the upper boundary, a'c', places this boundary at twice the Blasius boundary layer thickness [14]. The downstream boundary was located at multiples of the distance at which the slope of the Blasuis boundary layer is 0.01.

The boundary conditions for the Navier-Stokes equations in the transformed plane are as follows:

on a'b' (plate surface): $\psi = \psi_\eta = 0$ ($v = u = 0$, no-slip condition).

on a'c' (upper boundary); $\psi_\eta = \frac{1}{x_\xi}(J + x_\eta \psi_\xi)$, $\omega = 0$ ($u = 1$, $\omega = 0$, free stream conditions).

on b'c' (downstream boundary):

$$\psi = 2\left(\frac{t}{R}\right)^{\frac{1}{2}} \int_0^{\frac{y}{2\sqrt{\frac{t}{R}}}} \text{erf } \eta \, d\eta,$$

$$\omega = -\left(\frac{R}{\pi t}\right)^{\frac{1}{2}} \exp\left(-\frac{Ry^2}{4t}\right)$$ (infinite plate solution, Schlichting [14])

on a'a' (leading edge): $\psi = \omega = 0$.

The condition on the downstream boundary, b'c', is the exact solution of the Navier-Stokes equations for a suddenly accelerated fully infinite flat plate. The numerical quadrature was done by trapezoidal integration. The condition on ψ_η on the upper boundary expresses $u = 1$, the free stream velocity. All these boundary conditions were implemented directly except the $\psi_\eta = 0$ condition on the plate, a'b', which was satisfied by adjusting the value of the vorticity at each point on the body by the false-position iteration procedure discussed above.

The coordinate system used for the semi-infinite plate, shown in Fig. 3, has a curved boundary located at twice the Blasuis boundary layer thickness

above the plate, with coordinate lines coming to a point at the leading edge. This form was chosen in preference to systems with rectangular boundaries in order to concentrate the coordinate lines near the plate to a greater degree as the Reynolds number increases and also to ensure a test of a representative non-orthogonal curvilinear system.

Velocity profiles obtained using this coordinate system are shown in Fig. 4 and compared therein with the Blasius boundary layer solution (Schlichting [14]). (Positions are given in fractions of the distance to the downstream boundary.) Since the downstream boundary condition was the time-dependent solution for the completely infinite plate, for which the boundary layer thickness increases without bound as time increases, the agreement with the Blasius solution deteriorates as expected as this boundary is approached (position 1.0 in these figures). The loss of flow in the lower portion of the boundary layer that results from this continual thickening of the boundary layer on the downstream boundary causes the over-shoot of the Blasius profile that occurs upstream of this boundary. The agreement with the Blasius profile in regions farther removed from the downstream boundary is good. Note that the profiles upstream cling to the Blasius as the downstream profile moves away.

Coordinate system control was used to cause the system to expand down the plate. The agreement with the Blasius solution extends very near the leading edge, since the coordinate lines are more closely spaced near the leading edge. With the Blasius boundary layer solution as the downstream boundary condition the problem becomes a steady-state problem, and the agreement with the boundary layer solution is excellent, except at the first few steps near the leading edge [1], [5].

VI. SUBMERGED HYDROFOIL SOLUTION (Ref. [2])

Figure 5 shows the basic doubly-connected transformation with a free surface. This type of configuration has been used successfully for airfoils in previous studies [4]. For a free surface problem C_1 would be the arbitrary hydrofoil, C_2 would be the "infinity" boundary, and C_5 would be the free surface. Since the "infinity" boundary is chosen to be ten chords from the hydrofoil in the present research, the contour C_5 would be approximately twenty chords long. Thus, fewer points would be on C_5 to cover 20 chord lengths than would be on C_1 to cover approximately 2 chord lengths. Unless many ξ-points were used the wide grid spacing on the free surface would cause large truncation error.

Several modified coordinate systems were investigated in order to provide more points on the free surface [2].

Figure 6 shows the transformation that was used in this research. This coordinate transformation was chosen because the number of free surface (C_7 and C_8) grid points is independent of the number of points on the body (C_1). Also, no points with zero Jacobians occur on the free surface.

The transformed plane of Figure 6 forms a T-shaped region. The lower part of the coordinate system is the same as the basic transformation of Figure 5. The cut C_1^* is taken at $I1 - \frac{1}{2}$ $(I2 + \frac{1}{2})$, thus creating the two common reentrant boundaries C_3^* and C_4^*. The upper part of the transformed plane bounded by the constant η-line $(JM - \frac{1}{2})$ C_8, C_7, C_2 is added to the basic transformed plane to provide free surface and "infinity" boundaries. The two common reentrant boundaries C_6 and C_5 are created to provide more points on the infinity boundary than are on

the body (C_1^*). The cuts are taken at half indices because the point (I1 - $\frac{1}{2}$, JM - $\frac{1}{2}$) has a zero Jacobian. By taking the cut at half indices, the zero Jacobian point is eliminated from the field calculations.

The system of finite difference equations is solved simultaneously by the successive-over-relaxation (SOR) iterative method. The number of simultaneous equations to be solved is (JMAX - JM + 1)(IMAX - 1) + (JM - 1)(I2 - I1 + 1). Boundary values are specified on J = JMAX for all $i\varepsilon[1, IMAX]$. Also, boundary values are specified on j - JMAX for all $i\varepsilon[I1, I2]$. Boundary values or the Neumann boundary condition x_ξ = 0 (normal η-lines to free surface) may be expressed on the free surface contours, i = 1 and i = IMAX. At the branch cut for the constant η-line J = JM and $i\varepsilon[1, I1 - 1]$, we have

$$(i, j - 1) = (IMAX - i + 1, JM) .$$

Also, at the branch cut for the constant η-line J = JM and $i\varepsilon[I2 + 1, IMAX]$, we have

$$(i, j - 1) = (IMAX - i + 1, JM) .$$

At the branch cut for the constant ξ-line i = I1 and $j\varepsilon[1, JM - 1]$, we have

$$i - 1 = I2 .$$

At the branch cut for the constant ξ-line i = I2 and $j\varepsilon[1, JM - 1]$, we have

$$i + 1 = I1 .$$

The basic hydrofoil geometry and coordinates are shown in Figure 7. L is the chord length of the hydrofoil used, h is the depth of the water from the bottom to the undisturbed free surface, d is the depth of the hydrofoil below the free surface. U_∞ is the reference velocity for the problem (usually the steady-state free stream velocity), ν is the kinematic viscosity, ρ is the density, D is the incompressible continuity equation, and g is the local gravitational constant.

The equations of motion are those given in Section III except that the non-conservative form of the convective terms in the Navier-Stokes equations was used for this solution.

Typical results of the numerical solution are given in Figures 8-18 for a Karman-Trefftz hydrofoil (Figure 8) and in Figures 19-20 for a circular cylinder hydrofoil. The airfoil is defined by 37 coordinate points and is located one chord below the free surface. The field sizes of the coordinate grid are 54 x 30 and 54 x 60. The 54 x 60 field has its "outer" boundary located 20 chords from the airfoil, and the 54 x 30 field has its "outer" boundary located 10 chords from the airfoil. Using Figure 6, JM = 6, I1 = 10 and I2 = 45. Six η-lines were attracted to the airfoil with an amplitude of 1000 and a decay factor of 1.0.

Figure 9 shows the effect of Froude number on the free surface movement. Three Froude numbers of 0.5, 1.0 and 2.0 are shown for a constant Reynolds number of 20 and at a time of 8.0. All three cases were accelerated gradually over a time of 4.0. Also, the same time step size (Δt = .01) was used in all three cases. At a time of 8.0 the

airfoil had moved 4 chords at the free stream velocity of one. By comparing Figures 9a, b, and c, the effect of the airfoil on the free surface increases as the Froude number increases. This result is to be expected since the Froude number is the ratio of inertial forces to gravitational forces. Therefore, as the Froude number increases the inertial forces increase.

Figures 10, 11, and 12 demonstrate the effect of Froude number on the drag, lift, and pressure. The time histories (Figure 10) of drag for the three Froude numbers of 0.5, 1.0 and 2.0 are presented for Re = 20 and t = 8.0. Referring to the peak drag for each figure, the drag is reduced as the Froude number is increased, because as the Froude number increases the free surface rises over the airfoil which changes the local angle of attack. From Figure 11, the lift changes drastically because as the Froude number decreases the buoyancy forces become more dominant. From Figure 12 the effect of Froude number on the pressure distribution can be seen. Buoyancy forces are dominant at a Froude number of 0.5 (Figure 12b), and inertial forces are dominant at a Froude number of 2.0 (Figure 12d).

Figure 13 shows three time slices of a coordinate system. The airfoil is accelerated to the free stream velocity over a time period of 4. The flow parameters are F = 1.0 and Re = 20, and the airfoil is located one chord below the free surface. At t = 2.0, the airfoil has achieved half its free stream velocity. The airfoil movement has caused the free surface to rise slightly in front of the airfoil, and to sink slightly behind the airfoil. At t = 4.0, the airfoil has achieved the free stream velocity of 1.0. The free surface peak has moved to about the

quarter chord of the airfoil, and the lowest point on the free surface has moved one chord behind the airfoil. At t = 6.0, the airfoil has moved 2 chords at a constant velocity of 1.0. The first peak has remained at the quarter-chord, and the lowest peak has moved to about two chords behind the airfoil. Also, a second peak has begun to form downstream.

Figure 14 shows the velocity vector field at the three times of the previous figure. The figure shows the change in the angle of attack on the airfoil, due to the free surface movement, as time increases. The velocity at the trailing edge shows that the fluid leaves the trailing edge smoothly creating a wake behind the airfoil. The value of continuity at the trailing edge was the largest value in the field. Due to the low Reynolds number, the boundary layer is very thick.

Figure 15, shows the pressure distribution at three time steps. The figure shows the dominance of the inertial forces increasing over the buoyancy forces as time increases from 2 to 6.

Figures 16 and 17 show the effect of Reynolds number on the free surface at a constant Froude number and constant time. Figure 16 shows two coordinate systems, one at a Reynolds number of 20 and the other at a Reynolds number of 100. The Re = 100 case has less effect on the free surface than does the Re = 20 case. The effect of the Reynolds number on the free surface is due to the smaller boundary layer on the airfoil for a Reynolds number of 100 than for a Reynolds number of 20.

Figure 17 shows the pressure distributions about a Karman-Trefftz airfoil for two Reynolds numbers, Re = 20 and Re = 100. The constant parameters are F = 0.5 and t = 6. The pressure coefficients for Re =

20 are larger than the pressure coefficients for Re = 100. The lift coefficient for both cases is due mainly to the buoyancy forces. Figure 18 shows a velocity vector field for a Karman-Trefftz airfoil, Re = 100, F = 0.5, and t = 6. The boundary layer is shown to be smaller on the airfoil than in the Re = 20 case. The trailing edge wake is well defined.

Figures 19 and 20 show the versatility of the coordinate transformation. Figure 19 shows the coordinate system for a circular cylinder located one chord below the free surface. Three times are shown. The flow parameters are Re = 20 and F = 0.5 at a time of 6. Two wave peaks are shown on the free surface. The circular cylinder affects the free surface more than the airfoil, which should be expected. Figure 20 shows the velocity vectors for the circular cylinder of Figure 19. At a time of 6, the stagnation point started to move up the front of the cylinder.

Results are presented in Figures 21-23 for a hydrofoil in pitching, plunging, and longitudinal oscillation. All solutions are presented in the free stream-fixed coordinate reference frame. Also all solutions were run using the flow parameters, Re = 20 and F = 1.0. The same coordinate system was used for all solutions. A Karman-Trefftz airfoil was placed at one chord below the free surface. The infinity boundary was located 10 chords from the airfoil.

In Figure 21, the airfoil is moving in the negative x-direction. This solution is equivalent to the other solutions of previous sections. However, the hydrofoil is moving relative to the "outer" boundary. The coordinate lines close to the body are moving with the airfoil. The free stream-fixed reference frame clearly shows the fluid being pushed by the airfoil.

Also, fluid is moving in at the trailing edge to fill the space evacuated by the airfoil.

In Figure 22, the airfoil is moving toward the free surface. As the airfoil moves toward the free surface, fluid is pushed up and to the sides. Vortices are created at the leading edge and at the trailing edge of the airfoil because the fluid is moving from the upper side to the lower side. The fluid that is moved up by the airfoil disturbs the free surfaces by pushing up the free surface above the airfoil.

In Figure 23, the airfoil is pitching 5° about its center chord. Three times (t = 1, 5, 8) are shown. The airfoil takes a time of 10 to pitch from 0° to 5° and back to 0°. The vortices can be seen forming as the airfoil pitches.

Some of the solutions were generated on the UNIVAC 1106 single processor and the latest solutions were generated on the upgraded UNIVAC 1106 dual processor. There are many factors which determine the computer time required for a solution, for example, the way the object program is loaded in the computer code. Several examples of time required to solve the coordinate system and Navier-Stokes equations are presented.

The uncontracted coordinate system requires from 3 to 6 minutes to converge depending on the field size and convergence criteria. Depending on the type of attraction required, the contracted coordinate system takes up to 30 minutes.

Two similar solutions were generated with field sizes of 54 x 30 and 54 x 60. The acceleration parameter for pressure was 1.8 and the acceleration parameter for velocity was .8. The constant of .1 was used in the pressure iteration on the body. The flow parameters were Re = 20 and F = 1. The 54 x 30 solution took 239 minutes to generate 600 time steps and the 54 x 60 solution took 452 minutes to generate 600 time steps. The maximum number of iterations for a time step to converge was 11 at time step 313 for the 54 x 30 field. For the 54 x 60 field the maximum number of iterations was 12 at time step 304.

VII. HYDROFOIL IN FREE SURFACE SOLUTION (Ref. [3])

The physical and transformed planes used in this solution are shown in Figure 24. Since the hydrofoil is in the free surface, rather than submerged, the physical region is simply-connected, its boundaries being the wetted portion of the hydrofoil contour, ② - ③, the free surface fore, ① - ②, and aft, ③ - ④, and a remote semi-circular boundary, ① - ④, located at a sufficient distance from the hydrofoil to be undisturbed by the flow. The transformed plane is a rectangle, with the wetted portion of the hydrofoil contour transforming to the upper horizontal side, the free surface fore and aft transforming to the left and right vertical sides, respectively, and the semi-circular remote boundary transforming to the lower horizontal side as indicated in Figure 24. This configuration differs from that used for the submerged hydrofoil in that the physical region was doubly-connected with the submerged body.

As noted above, the curvilinear coordinates (ξ,η) are taken as the solution of two elliptic partial differential equations. The particular equations used in the present solution are those of [15], which differ from the original system of [9], used for the submerged hydrofoil, only in the form of the coordinate system control terms (the terms involving the functions P and Q below and in Eq. (2) above.) Thus ξ and η are determined by the solution of

$$\xi_{xx} + \xi_{yy} = (\xi_x^2 + \xi_y^2)\ P(\xi,\eta) \tag{17a}$$

$$\eta_{xx} + \eta_{yy} = (\eta_x^2 + \eta_y^2)\ Q(\xi,\eta) \tag{17b}$$

With reference again to Figure 24, the boundary conditions for these equations are as follows:

(a) on the wetted portion of the hydrofoil contour, ② - ③:

$\eta = \eta_2$ = constant, ξ varying monotonically from ξ_1 to ξ_2 ($\xi_2 > \xi_1$) from ② to ③

(b) on the free surface, ① - ②, and ③ - ④:

$\xi = \xi_1$ = constant on ① - ②, $\xi = \xi_2$ = constant > ξ_1 on ③ - ④,

η varying monotonically from η_1 to η_2 ($\eta_2 > \eta_1$) from ① to ② and from ④ to ③.

(c) on the remote boundary, ① - ④.

$\eta = \eta_1$ = constant < η_2. ξ varying monotonically from ξ_1 to ξ_2 from ① to ④.

The coordinate control functions, $P(\xi,\eta)$ and $Q(\xi,\eta)$ serve to concentrate coordinate lines as desired to resolve expected large gradients. The theory and use of such control has been discussed in some detail in [9]. In the present application, these functions are determined from the specified spacing of points on the hydrofoil contour and free surface, those on the body being concentrated near the free surface and those on the surface being concentrated near the hydrofoil as in Figure 25. The details of this determination of P and Q are given in Reference 3. The resultant concentration of coordinate lines near the body and free surface is evident in Figure 25.

In the initial stages of this study, the control functions, P and Q, were taken as sums of decaying exponentials that cause attraction of coordinate lines to specified lines and/or points as used for the submerged hydrofoil. Some of the results given below were obtained on coordinate systems using this type of control as will be noted. The new control

procedure has the advantage of automating the control and eliminating the need for judgmental estimation of the attraction amplitudes and decay factors necessary to achieve a desired degree of line concentration.

With the current modification in the control functions, Eq. 2 in the transformed plane are replaced by

$$\alpha x_{\xi\xi} - 2\beta x_{\xi\eta} + \gamma x_{\eta\eta} + \alpha P x_{\xi} + \gamma Q x_{\eta} = 0 \qquad (18a)$$

$$\alpha y_{\xi\xi} - 2\beta y_{\xi\eta} + \gamma y_{\eta\eta} + \alpha P y_{\xi} + \gamma Q y_{\eta} = 0 \qquad (18b)$$

The boundary conditions for x and y are as follows:

(a) On the hydrofoil:

x and y specified by the chosen spacing of points around the hydrofoil contour. These points move on the contour with time as a result of motion of the hydrofoil and also because of movement of the free surface-body contact points on the contour.

(b) On the free surface:

$x_{\xi} = 0$ initially, fixed thereafter, y from the surface movement, Eq. (10). (The first of these allows the points to slide along the free surface so that the coordinate lines are initially vertical at the free surface.)

(c) On the remote boundary:

x and y fixed and specified by the chosen spacing of points along the remote boundary.

This point distribution on the body and remote boundary was taken according to equi-angular spacing over the body and remote boundary arcs in the earlier stages of the present investigation. Later an unequal

spacing was used, with the angular separation of points varying on a sine curve, so that the closest spacing occurs adjacent to the free surface.

Since the free surface deforms in time, with consequent motion of its intersections with the hydrofoil contour, only the relative distribution of points on the hydrofoil contour is kept fixed. The points thus slide along the wetted portion of the hydrofoil while maintaining the same relative spacing from adjacent points as time progresses. This is accomplished by locating the points on the contour at fixed percentages of the angle subtended by the arc between the two intersections with the free surface. This subtended angle, of course, changes in time. When the hydrofoil oscillates, the movement follows the oscillating motion of the body as well.

The points on the free surface are initially determined by a Neumann boundary condition that requires the coordinate lines to be vertical at the moving surface. The local elevation of the surface is determined by the equations of motion for the free surface as discussed in Section III. The points thus slide along the free surface as the surface deforms in time.

Results of the numerical solution are presented for a circular cylinder hydrofoil in two flow configurations:

(a) Accelerating translational motion parallel to the plane of the initially undisturbed flat free surface.

(b) Oscillatory plunging motion normal to the plane of the initially undisturbed flat free surface.

In each case the axis of the cylinder is in the plane of the initially undistrubed flat free surface. The fluid is physically unbounded except by the free surface, with no disturbance remote from the hydrofoil.

In the translational case (a) the acceleration is linear, with the Reynolds and Froude numbers given by

$$R = 20t \qquad\qquad F = 2t$$

these numbers being based on the cylinder diameter and current velocity.

For the plunging case the motion of the hydrofoil is sinusoidal with the elevation of the cylinder axis relative to the plane of the initially undisturbed free surface given by

$$y = A \sin(\frac{2\pi t}{P})$$

where A and P are the amplitude and period, respectively, of the motion. The velocity of the cylinder is thus

$$\dot{y} = \frac{2\pi A}{P} \cos(\frac{2\pi t}{P})$$

and the Reynolds and Froude numbers are then given by $R = 20\dot{y}$ and $F = 2\dot{y}$, respectively.

In each case the coordinate system is of the form shown in Figure 25 and discussed above in this section, with 37 points on the body and 30 points on the free surface on each side of the body. The remote boundary where the fluid is undisturbed is located at a radius of 10 cylinder diameters. The convergence acceleration parameters used were 1.0 for the momentum equations (7a-b), 1.8 for the Poisson equation (7c), 0.45 for the surface pressure equation (9), and 1.85 for the coordinate system equations (18). The iterative convergence criteria used were 10^{-5} for the coordinate system and 10^{-4} for the velocity and pressure.

The initial point distribution on the cylinder was determined by a sine curve, with points distributed symmetrically and concentrated near each free surface contact point. The initial distribution on the free surface was determined by an exponential curve, with points concentrated near the body. It was found necessary to have the points adjacent to the free surface-body contact point approximately equidistant from the contact point else stability problems arose with the surface. The points move on both the hydrofoil and free surface as time passes, but the same relative distributions are maintained as discussed in the previous section.

As noted in the discussions above, the curvilinear coordinate system continually deforms as time progresses, always keeping a coordinate line coincident with the deforming free surface. This behavior is evident in Figure 25 which shows the coordinate system at four times for the translating hydrofoil. The free surface rises in front of the hydrofoil, and the fore contact point slides up along the hydrofoil contour. At the rear of the hydrofoil, the surface falls, and the aft contact point moves downward.

Velocity vectors and the hydrofoil pressure distribution for this solution are shown at one time in Figure 26. The vectors clearly show the fore and aft stagnation points to be well below the corresponding surface contact points on the hydrofoil. The pressure distribution shows a positive pressure spike adjacent to both contact points, but a smooth distribution elsewhere on the hydrofoil. This spike is due to numerical error resulting probably from the modeling of the contact point movement.

Figures 27 and 28 give the surface elevation and pressure distribution in the vicinity of the hydrofoil for three times. There is a smooth rise of the surface in front of the hydrofoil and a smooth depression behind. The low Reynolds number for this solution causes distributions to dissipate downstream so that no surface waves occur. The surface pressure distribution in Figure 28 shows some jaggedness just upstream of the hydrofoil. This is probably due to the numerical phenomenum of wiggles (two-cell wavelength oscillations), introduced in the present case by the modeling of the contact point where the pressure is fixed at zero.

The initially undeformed coordinate system used in the oscillatory solution is shown in Figure 29. A stronger concentration of lines near the free surface and hydrofoil contour was used in view of the results discussed above. Figure 30 shows the temporal oscillation of the lift coefficient. The curve is seen to be deformed from a pure sinusodial oscillation. After an initial rise, the force remains upward throughout the cycle.

Figure 31 shows a series of plots of velocity vectors at several times during the cycle, while Figure 32 shows the same thing but in detail of the region around the right surface-body contact point. As the body rises initially, the fluid moves downward from the surface and inward toward the void being left by the rising body (cf. T = 0.01 in Figure 31). Since the fluid adjacent to the body must rise with the body, however, due to the viscous no-slip boundary condition, a vortex is created near the contact point (T = 0.01 in Figure 32). (A similar vortex, but of the opposite rotation is, of course, created off the left contact point.) These vortices move away from the body and decrease in intensity as the quarter-cycle is approached (cf. T = 0.11 in Figure 32).

At the quarter-cycle (0.157), the body reaches its highest point and then reverses its motion to move downward. This forces the fluid beneath the body to the sides. The beginning of this sideward motion can be seen at T = 0.17 in Figure 31 just beneath the body. At this time, inertia causes most of the fluid to still reflect the previous upward movement of the body. This inertial effect is evident also in the corresponding detail plot in Figure 32, where the fluid adjacent to the body has reversed its motion and is moving downward with the body while the rest of the fluid motion is qualitatively similar to that at T = 0.15 before the quarter-cycle.

As time passes, the influence of the downward motion of the body spreads progressively throughout the fluid so that more and more of the fluid acquires downward and sideward motion beneath the body, with consequent upward motion toward the surface (cf. T = 0.21 and 0.31 in Figure 31). This annihilates the vortices, and new vortices of opposite rotation to the original form just off each surface-body contact point (cf. T = 0.21 in Figure 32.) These vortices also move away from the body and decrease in intensity as the body moves toward its lowest point at the three-quarter cycle time (T = 0.471).

At this time the motion of the body again reverses, and the body starts back upward. This causes inward motion to begin just beneath the body (T = 0.49 in Figure 31) with upward motion adjacent to the body (T = 0.49 in Figure 32). This new pattern of motion then spreads out into the remainder of the fluid, competing initially with the inertially persisting motion from before the last body reversal. As at the quarter-cycle, the existing vortices are annihilated, and new ones of opposite

rotation again form off the contact points (cf. T = 0.53 in Figure 32). The general fluid motion is again downward from the surface, with inward and upward motion beneath the rising body (cf. T = 0.61 in Figure 31) as at the beginning of the cycle.

The movement of the hydrofoil free surface contact points along the hydrofoil contour is modeled by a condition of continuity as discussed in detail in Ref. 3. Essentially this model causes the contact points to slide along the hydrofoil contour in response to a net inbalance of flow into the cell at the contact point. Net inflow will thus cause that contact point to slide upward along the contour. Another model based on a condition of zero stress at the contact point was also investigated but was found to be unsatisfactory as also discussed in Ref. 3.

Figures 33 and 34 show the surface elevation and pressure at approximately the quarter, half, three-quarter, and full cycle times. The elevation curves show that the mean surface position is not flat, but is depressed in the vicinity of the body. This result is in qualitative agreement with a periodic boundary layer solution and experimental flow visualization results given in Schlichting [14] for a circular cylinder oscillating in an unbounded fluid. There it is shown that a mean secondary motion exists in which fluid moves from the sides toward the body (normal to the direction of oscillation) and then away from the body parallel to the oscillation direction (cf. Figure 11.7 of [14]). In the present case this type of mean flow would be toward the body, parallel to the free surface, and then away from the surface beneath the body. This then would result in a mean surface depression.

VIII. CONCLUSION

The excellent comparison of the numerical results based on the technique of numerically-generated boundary-fitted coordinate systems with the Blasius boundary layer solution for the semi-infinite flat plate demonstrates that this technique can be quite useful in the numerical solution of the Navier-Stokes equations.

The technique of numerically generated boundary-fitted coordinate systems is clearly an effective aid in treating flow problems involving both free surfaces and solid boundaries. With this technique the complication of the boundary shape is essentially removed from the problem. It is possible to obtain numerical solutions for viscous flow, with viscous boundary conditions on the free surface as well as on the solid body.

The research results presented in this report leave several problems unresolved. Regarding the submerged hydrofoil solution, the coordinate configuration used had a zero Jacobian between grid points in the field of calculation. This zero Jacobian made it difficult to contract coordinate lines near the branch. Also, an ambiguity in the finite difference expressions for the cross derivatives at the point of zero Jacobian led to ambiguous results in the coordinate solutions. Thirdly, the coordinate control functions were found to be inadequate in controlling coordinate lines in the field. An arbitrary change in the coordinate control often led to unpredictable results for the physical coordinates. Some progress was made in this area during the latter stages concerning the hydrofoil in the free surface with the incorporation of an automated control. Finally, at project termination, the solution could not be run successfully for Reynolds numbers greater than 100 for the submerged hydrofoil. The combination of the coordinate contraction functions and the field point with a zero

Jacobian is believed to be the cause of a pressure source that occurred at the trailing edge of hydrofoils for Re > 100. Finally, since higher Reynolds numbers were not obtained, the method could not be verified with the experimental data available for submerged hydrofoils.

The presence of a zero Jacobian in the field is not a universal feature in the boundary-fitted coordinate systems, but is peculiar to the type of configuration adopted for the transformed plane in the submerged hydrofoil solution. This configuration did have certain advantages as noted in spite of the presence of the zero Jacobian. The configurations used for the hydrofoil in the free surface and for the semi-infinite flat plate (and for the external flow about airfoils in other studies) do not have any zeros of the Jacobian in the field. Further study would be necessary to develop better configurations for the submerged hydrofoil case.

Concerning the hydrofoil in the surface, the coordinate configuration was less of a problem, and no zeros of the Jacobian occurred in the field. The results given in the present work are all at very low Reynolds number, but the solution can in principle be run at any Reynolds number by increasing the attraction of the coordinate lines to the body and free surface at higher Reynolds numbers in order to maintain a sufficient number of lines in the viscous layers. Such a procedure is currently under investigation in connection with the flow about airfoils. The problem is made more difficult, however, with increasing Reynolds number. More investigation of the control of the coordinate system so that sufficiently close spacing is maintained near the free surface as it deforms is necessary, as is further study of the modeling of the hydrofoil-free surface contact point movement.

The inclusion of a bottom of arbitrary shape in the current solution is not difficult, nor would be the addition of a second hydrofoil in tandem. (The inclusion of a solid bottom was accomplished in an extension of the present work as reported in [16].) Similarly the hydrofoil and/or bottom could be allowed to deform in time without complicating the problem unduly. This is because all of the computation is done on the fixed rectangular transformed grid regardless of the shape or movement of the physical boundaries. Wind shear on the free surface could also be added by a change in surface boundary conditions to include applied external shear as well as pressure.

REFERENCES

1. Walker, R. L., "Numerical Solution of the Navier-Stokes Equations for Incompressible Viscous Laminar Flow Past a Semi-Infinite Flat Plate," M.S. Thesis, Mississippi State University, Mississippi State, Mississippi (1974).

2. Shanks, S. P., "Numerical Simulation of Viscous Flow about Submerged Arbitrary Hydrofoils using Non-orthogonal, Curvilinear Coordinates," Ph.D. Dissertation, Mississippi State University, Mississippi State, Mississippi (1977).

3. Thompson, J. F., and Shanks, S. P., "Numerical Solution of the Navier-Stokes Equations for 2D Surface Hydrofoils," EIRS-ASE-77-4, Mississippi State University, Mississippi State, Mississippi, (1977).

4. Thames, F. C., Thompson, J. F., et. al., "Numerical Solutions for Viscous and Potential Flow about Arbitrary Two-Dimensional Bodies using Body-Fitted Coordinate Systems," accepted for publication in Journal of Computational Physics (1976).

5. Thompson, J. F., Thames, F. C., Walker, R. L., Shanks, S. P., "Numerical Solutions of the Unsteady Navier-Stokes Equations for Arbitrary Bodies using Boundary-Fitted Curvilinear Coordinates," Proceedings of Arizona/AFOSR Symposium on Unsteady Aerodynamics, University of Arizona (1975).

6. Thompson, J. F., Thames, F. C., Shanks, S. P., Hodge, J. K., and Mastin, C. W., "Solutions of the Navier-Stokes Equations in Various Flow Regimes on Fields Containing any Number of Arbitrarily-Shaped Two-Dimensional Bodies using Boundary-Fitted Curvilinear Coordinate Systems," 5th International Conference on Numerical Methods in Fluid Dynamics, Enschede, the Netherlands (1976).

7. Thompson, J. F., Thames, F. C., and Mastin, C. W., "Automatic Numerical Generation of Body-Fitted Curvilinear Coordinate System for Field Containing any Number of Arbitrary Two-Dimensional Bodies," Journal of Computational Physics, 15, 299 (1974).

8. Thompson, J. F., Thames, F. C., Mastin, C. W., "TOMCAT - A Code for Numerical Generation of Boundary-Fitted Curvilinear Coordinate Systems on Fields Containing any Number of Arbitrary Two-Dimensional Bodies," accepted for publication in Journal of Computational Physics (1976).

9. Thompson, J. F., Thames, F. C., and Mastin, C. W., "Boundary-Fitted Coordinate Systems for Solution of Partial Differential Equations on Fields Containing any Number of Arbitrary Two-Dimensional Bodies," NACA CR-2729, 1977.

10. Hodge, J. L., "Numerical Solution of Incompressible Laminar Flow about Arbitrary Bodies in Body-Fitted Curvilinear Coordinates," Ph.D. Dissertation, Mississippi State University, Mississippi State, Mississippi (1975).

11. Hirt, C. W., and Harlow, F. H., "A General Corrective Procedure for the Numerical Solution of Initial Value Problems," Journal of Computational Physics, 2, 114 (1967).

12. Thames, F. C., "Numerical Solution of the Incompressible Navier-Stokes Equations about Arbitrary Two-Dimensional Bodies," Ph.D. Dissertation, Mississippi State University, Mississippi State, Mississippi (1975).

13. M. Israeli, "A Fast Implicit Method for Time Dependent Viscous Flows," Studies in Applied Math, 49, 327 (1970).

14. Schlichting, H., Boundary Layer Theory, 4th Ed., McGraw-Hill, (1960).

15. Warsi, Z. U. A., Thompson, J. F., "Machine Solutions of Partial Differential Equations in the Numerically Generated Coordinate System," MMSU-EIRS-ASE-77-1, Engineering and Industrial Research Station, Mississippi State University,(1977).

16. Thompson, J. F. and Shanks, S. P., "Numerical Solution of the Navier-Stokes Equations for Arbitrary 2D Submerged Hydrofoils in a Channel of Finite Depth." MMSU-EIRS-ASE-77-6, Mississippi State University, Mississippi State, Mississippi (1977).

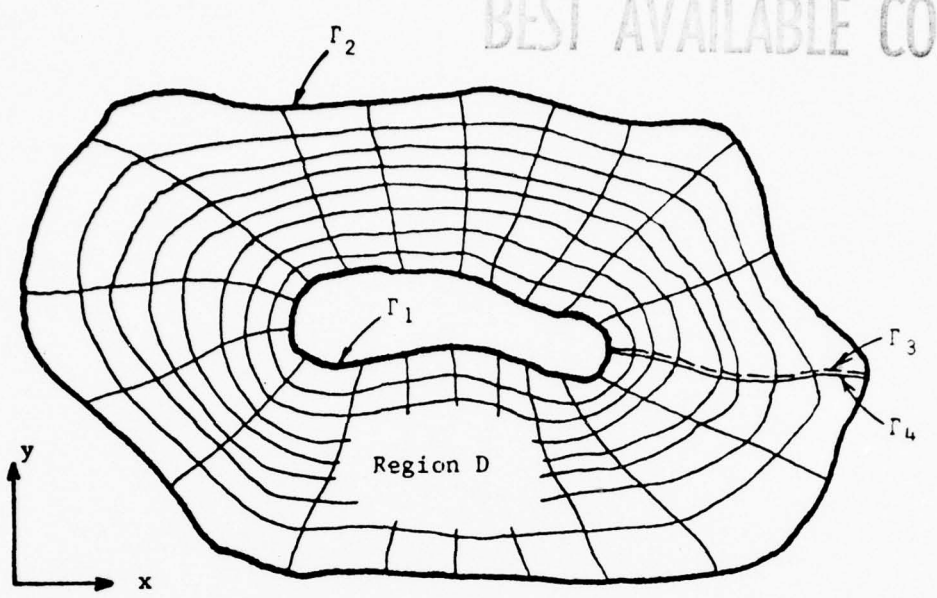

Physical Plane

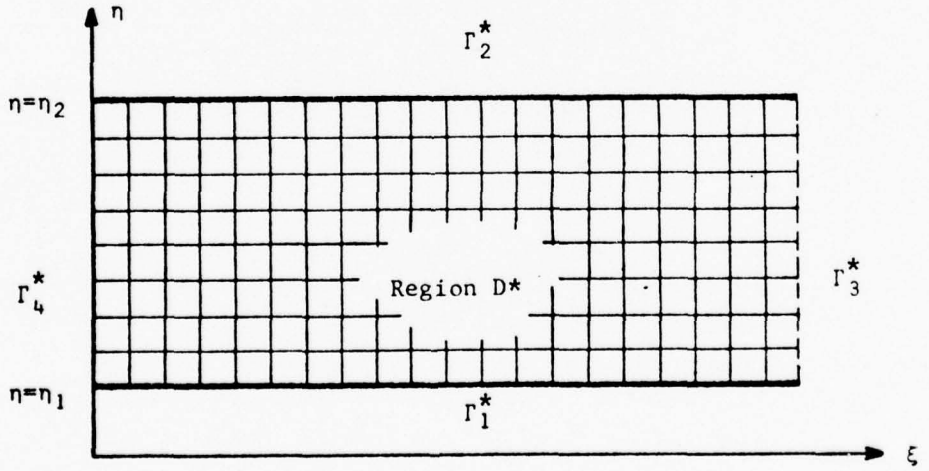

Transformed Plane

Figure 1. Field Transformation - Single Body

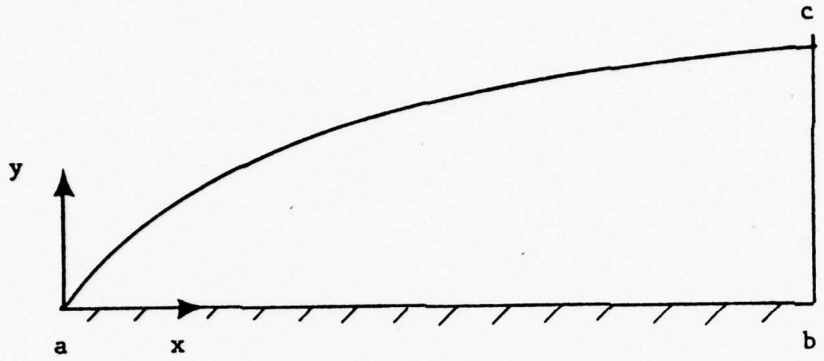

Physical Field

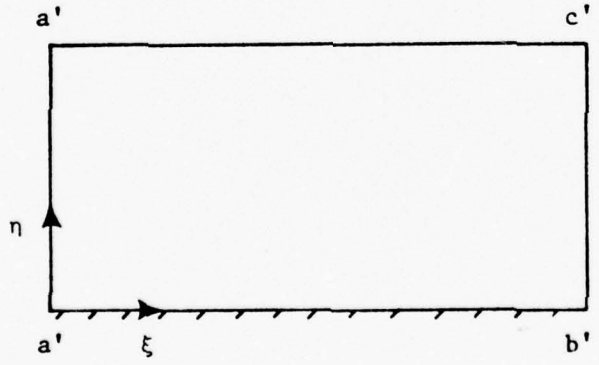

Transformed Field

Figure 2. Relation between Physical and Transformed Fields - Semi-Infinite Flat Plate

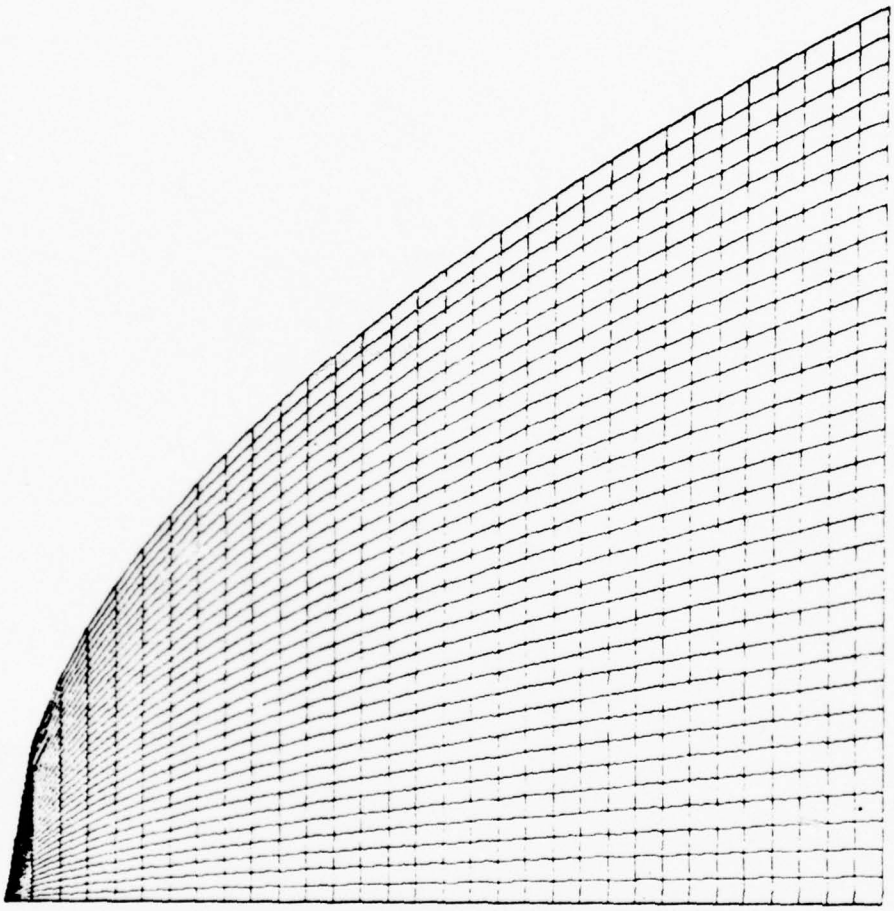

(a). Vertical Scale Exaggerated for Plot

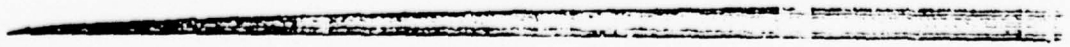

(b). Actual System

Figure 3. Coordinate System - Semi-Infinite Flat Plate

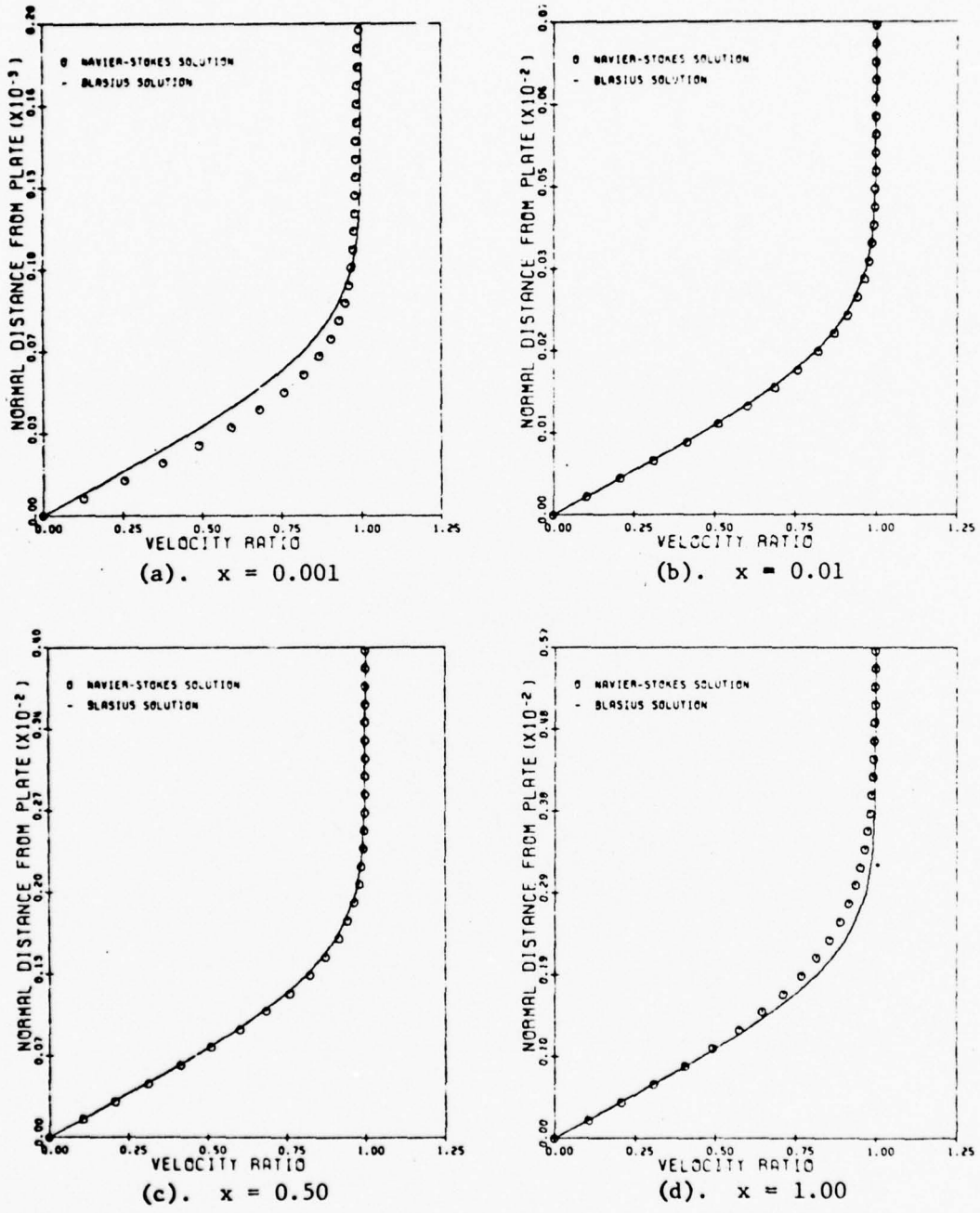

(a). x = 0.001 (b). x = 0.01

(c). x = 0.50 (d). x = 1.00

Figure 4. Semi-Infinite Flat Plate Solution. t = 1.24 (Downstream Boundary at Eight Times the Distance where Blasius Boundary Layer Slope is 0.01, XMAX = 0.45312)

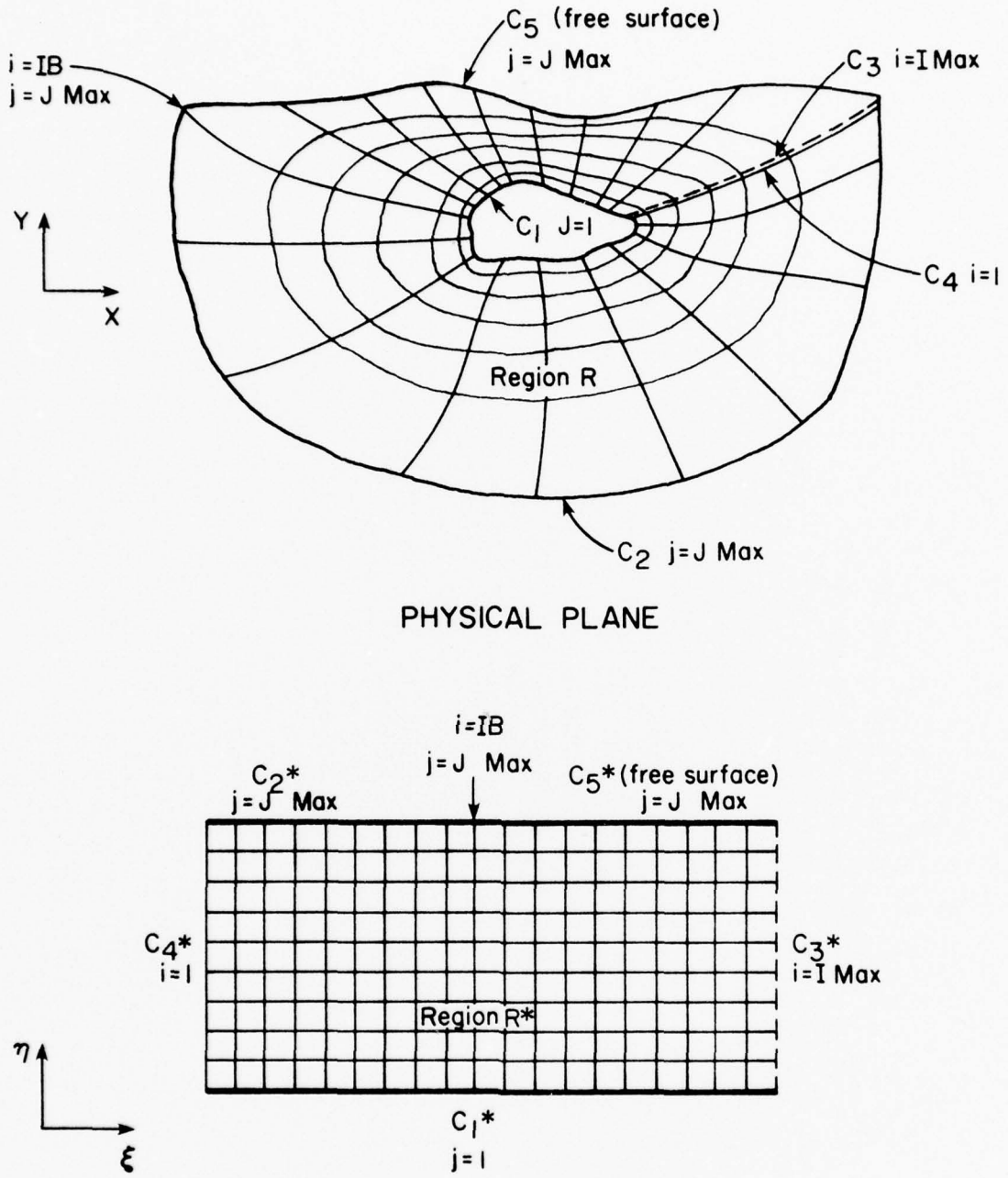

Figure 5. Doubly-Connected Region with Free-Surface

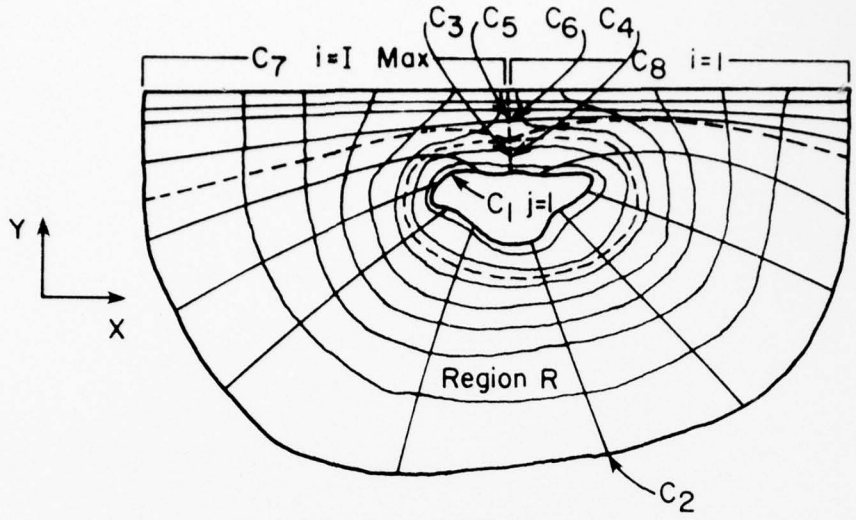

PHYSICAL PLANE

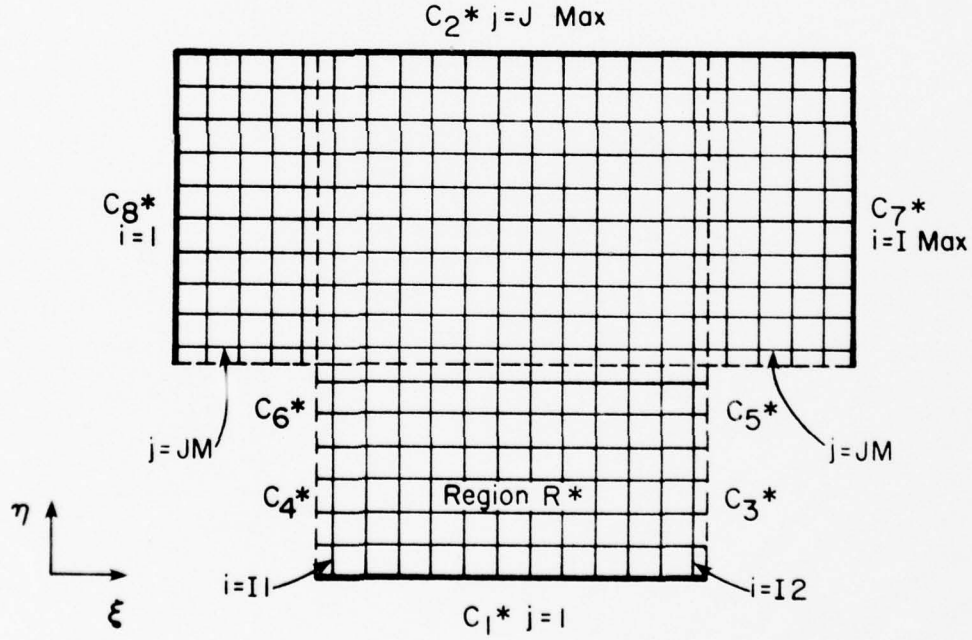

TRANSFORMED PLANE

Figure 6. Modified Doubly-Connected Region with Free-Surface

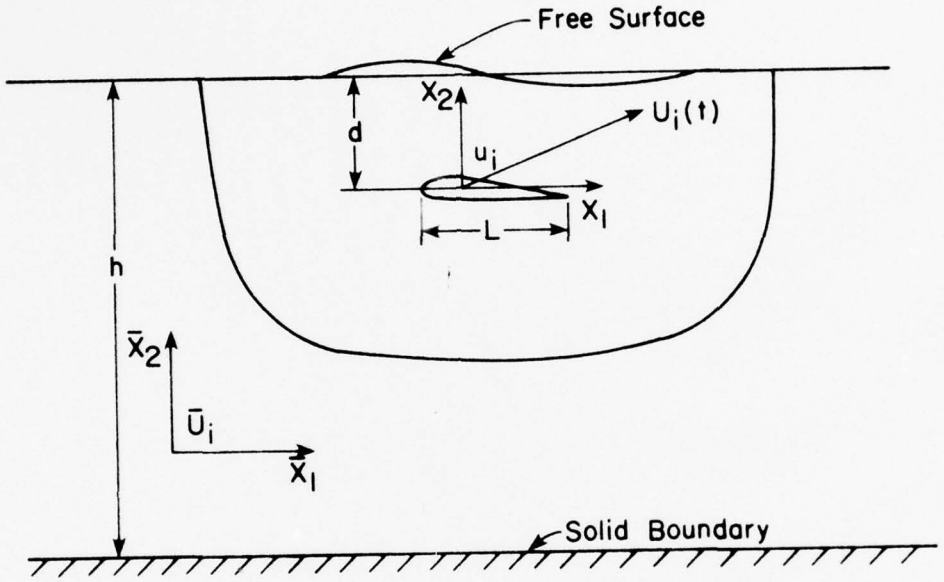

Figure 7. Hydrofoil Geometry and Coordinates

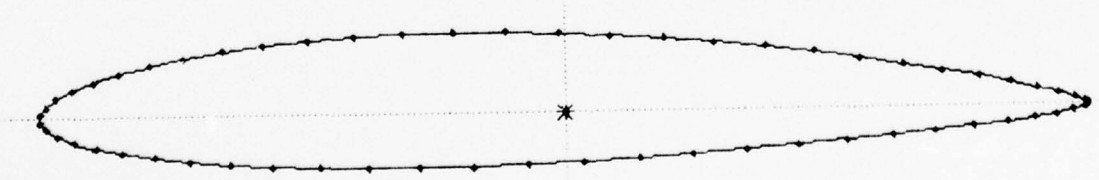

Figure 8. Karman-Trefftz Airfoil

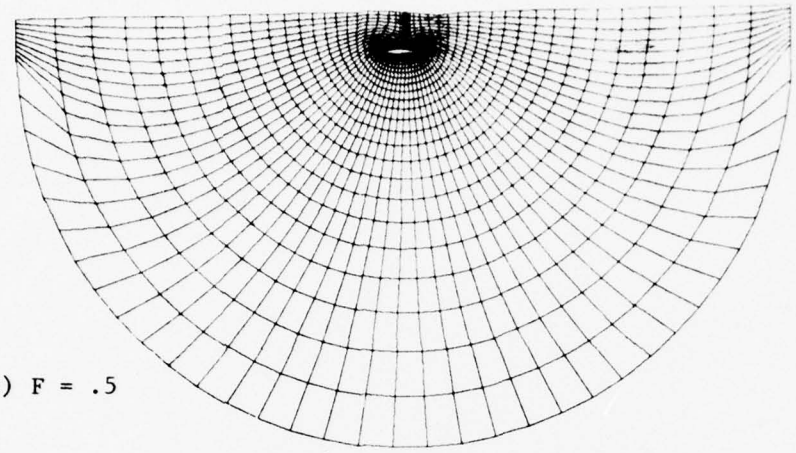

(a) F = .5

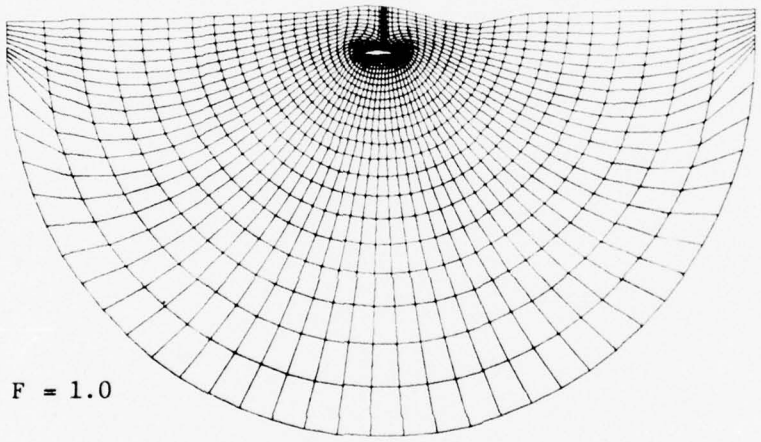

(b) F = 1.0

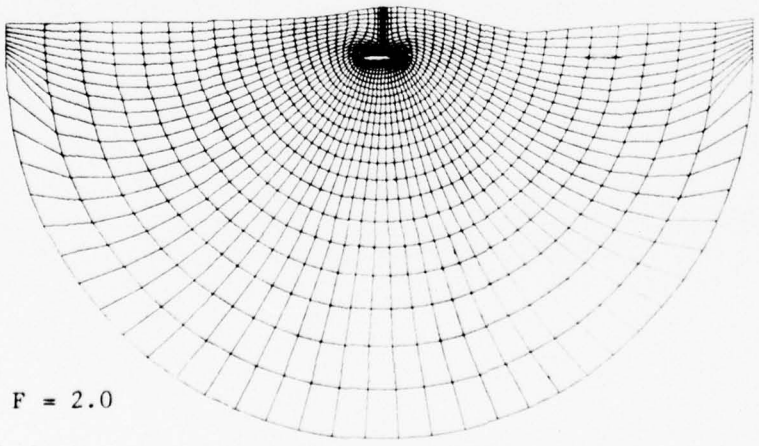

(c) F = 2.0

Figure 9. Coordinate system for three froude numbers, Re = 20, t = 8.0 - Karman-Trefftz Airfoil located 1 chord below free surface.

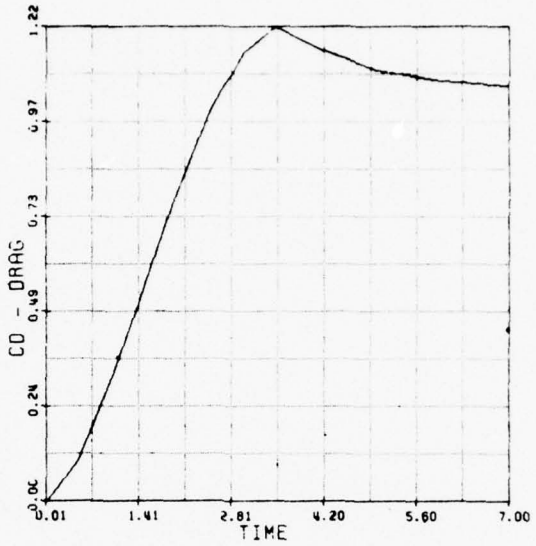

(a) F = 0.5

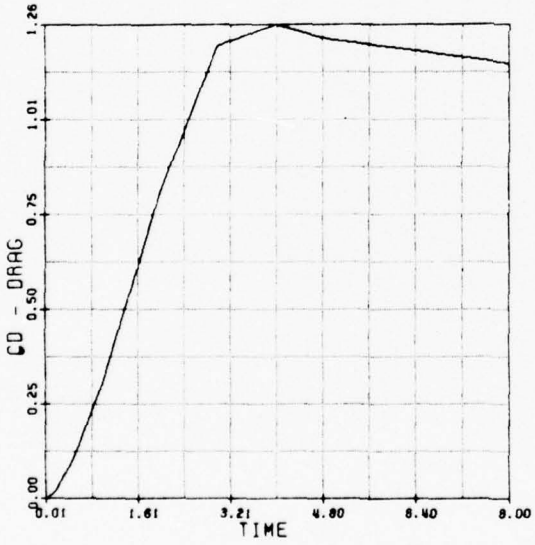

(b) F = 1.0

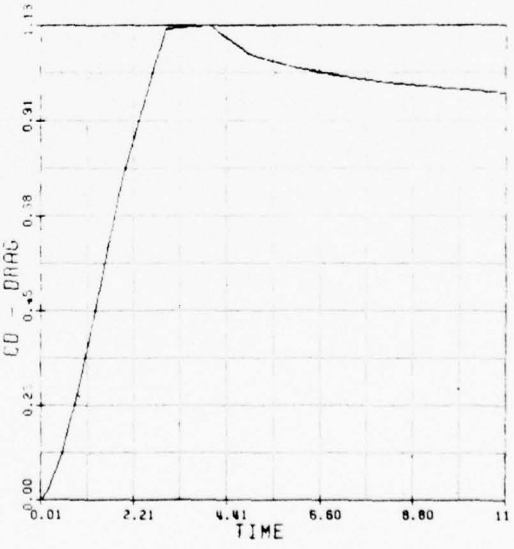

(c) F = 2.0

Figure 10. Time histroy of drag for three Froude numbers, Re = 20 - Karman-Trefftz Airfoil located 1 chord below free surface.

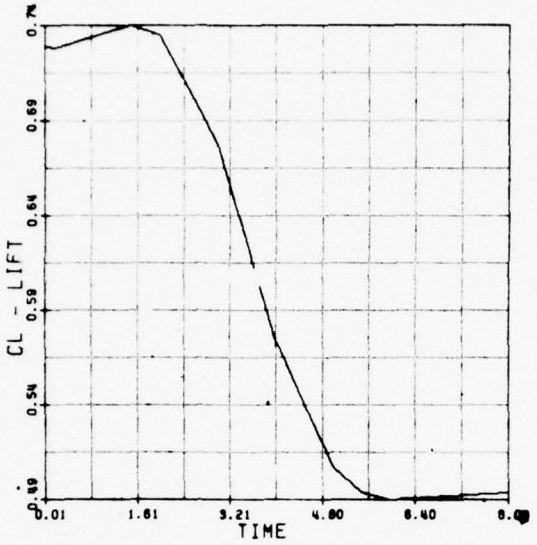

(a) F = 0.5

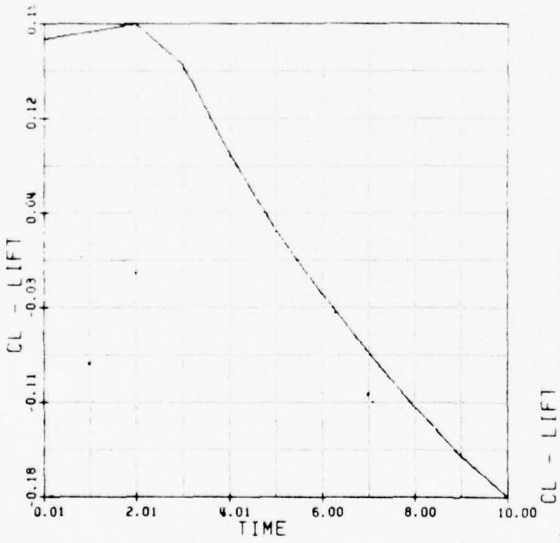

(b) F = 1.0

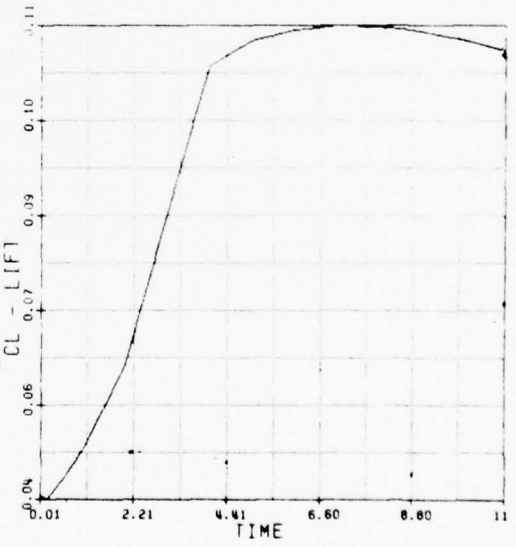

(c) F = 2.0

Figure 11. Time history of lift for three Froude numbers, Re = 2.0 - Karman-Trefftz Airfoil located 1 chord below free surface.

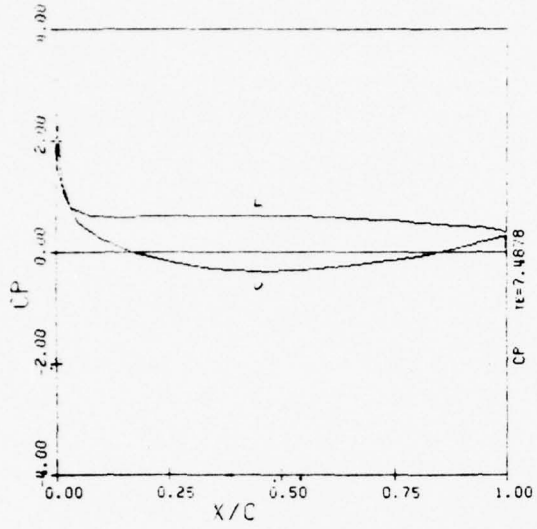

(a) F = 0.5, Re = 100

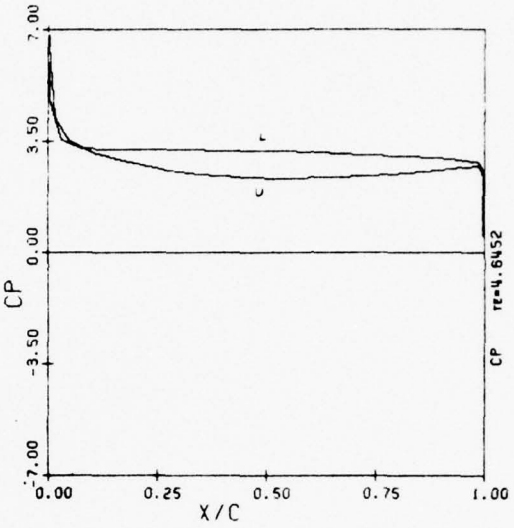

(b) F = 0.5, Re = 20

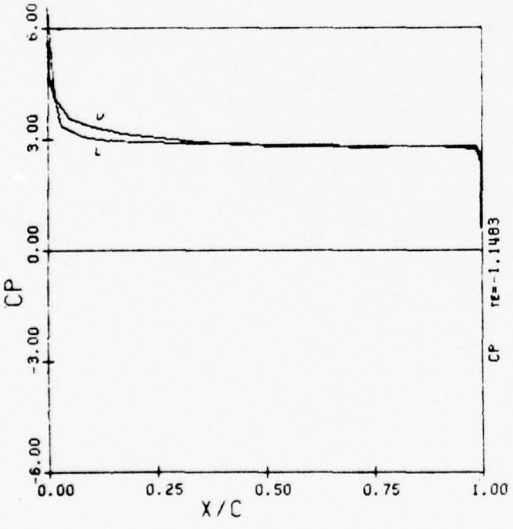

(c) F = 1.0, Re = 20

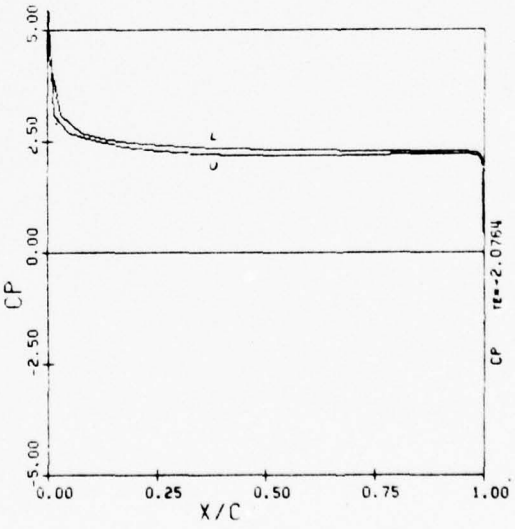

(d) F = 2.0, Re = 20

Figure 12. Pressure distribution for various Reynolds and Froude numbers at t = 8.0 - Karman-Trefftz Airfoil located 1 chord below free surface.

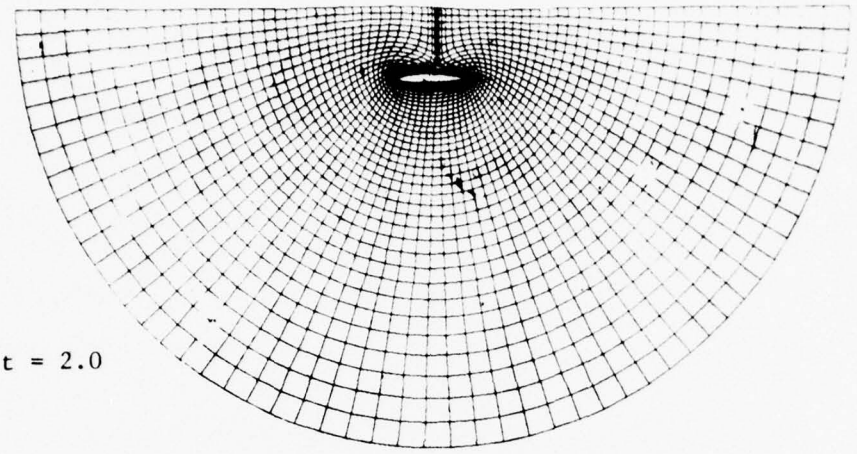

(a) t = 2.0

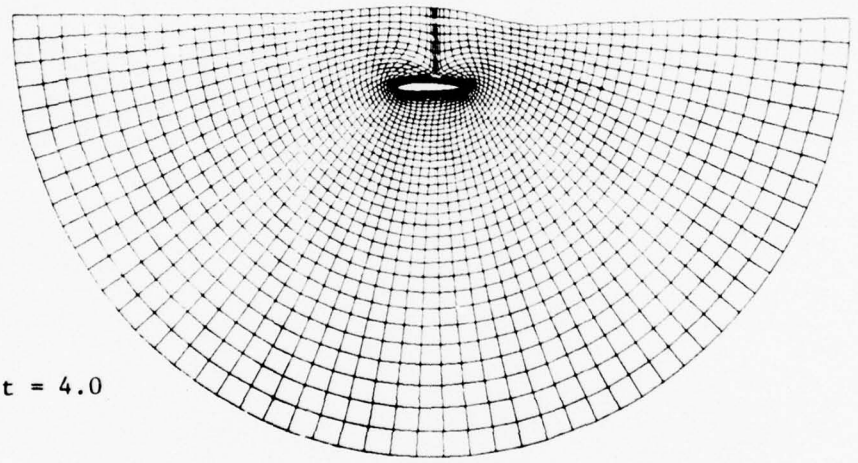

(b) t = 4.0

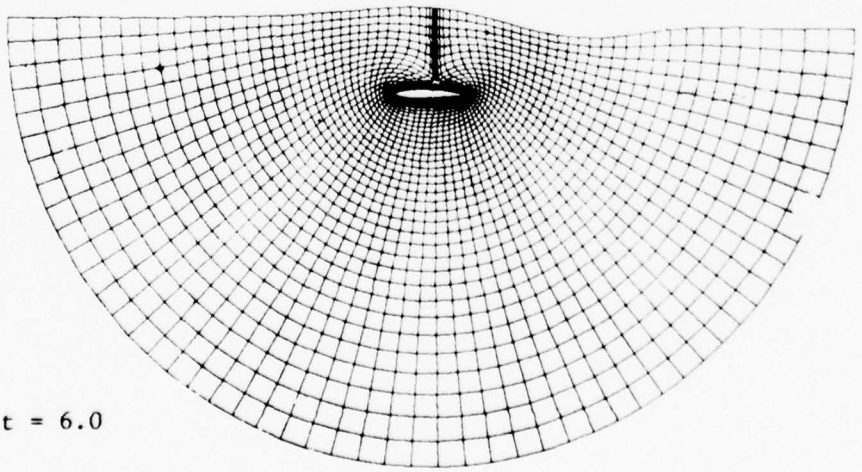

(c) t = 6.0

Figure 13. Coordinate system at three times, F = 1.0, Re = 20-Karman-Trefftz Airfoil located 1 chord below free surface.

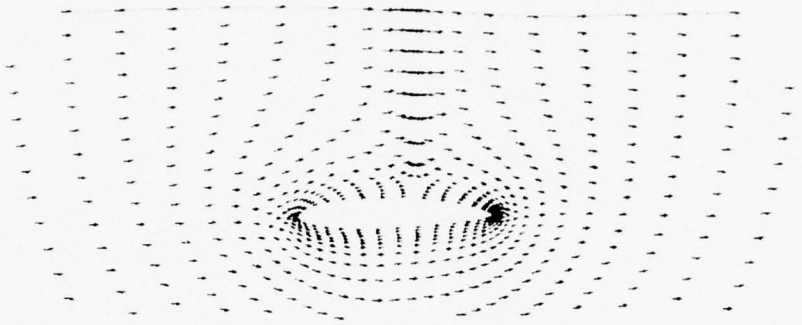

(a) t = 2.0

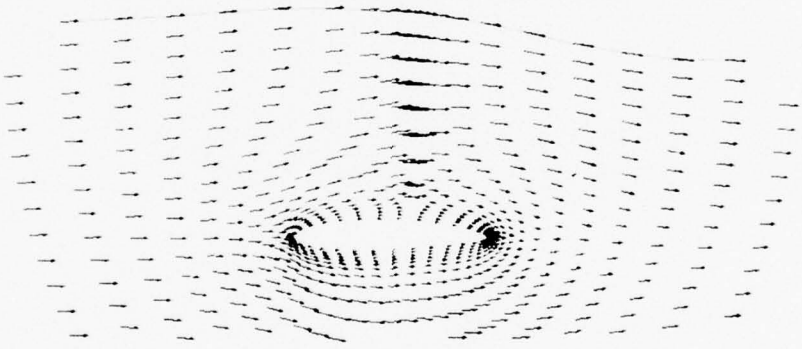

(b) t = 4.0

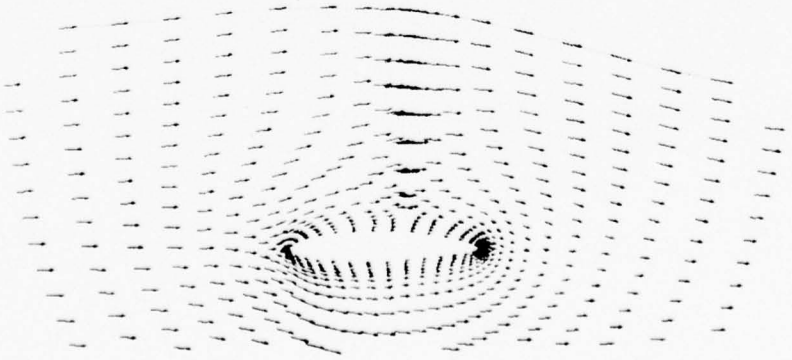

(c) t = 6.0

Figure 14. Velocity vector field at three times, F = 1, Re = 20 - Karman-Trefftz Airfoil located 1 chord below a free surface.

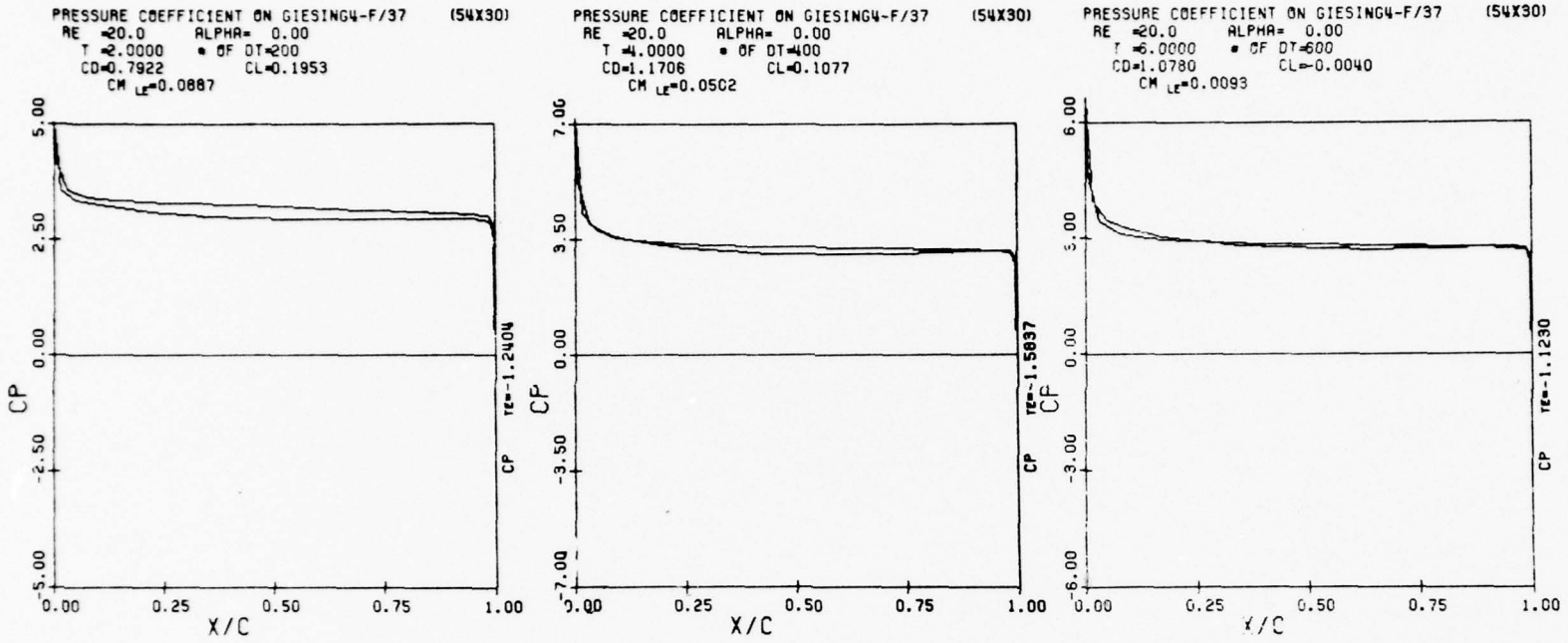

(a) t = 2.0 (b) t = 4.0 (c) t = 6.0

Figure 15. Pressure distribution at three times, F = 1.0, Re = 20 - Karman-Trefftz Airfoils located 1 chord below a free surface.

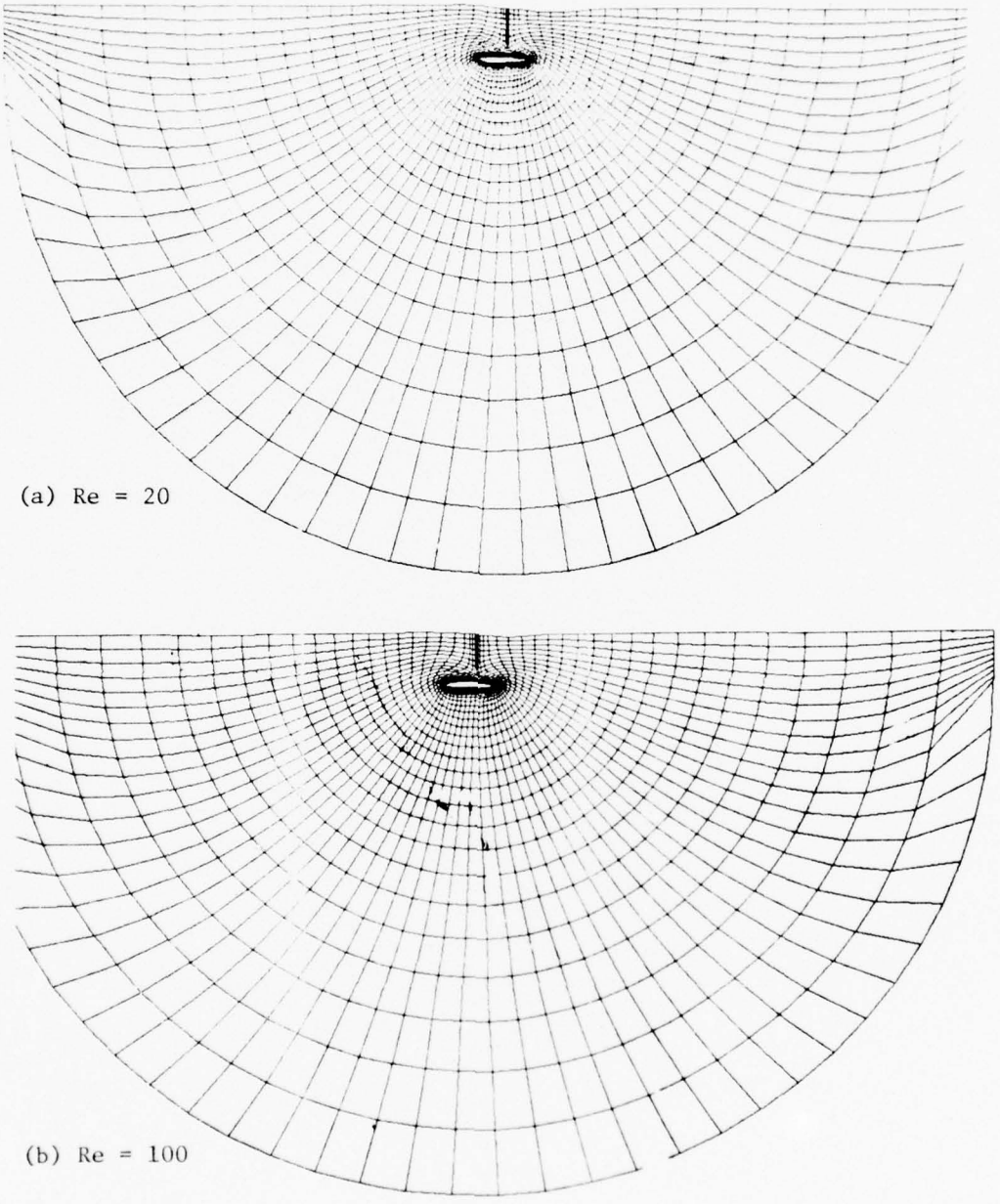

(a) Re = 20

(b) Re = 100

Figure 16. Coordinate system for two Reynolds numbers, F = 0.5, t = 6.0 - Karman-Trefftz Airfoil located 1 chord below a free surface

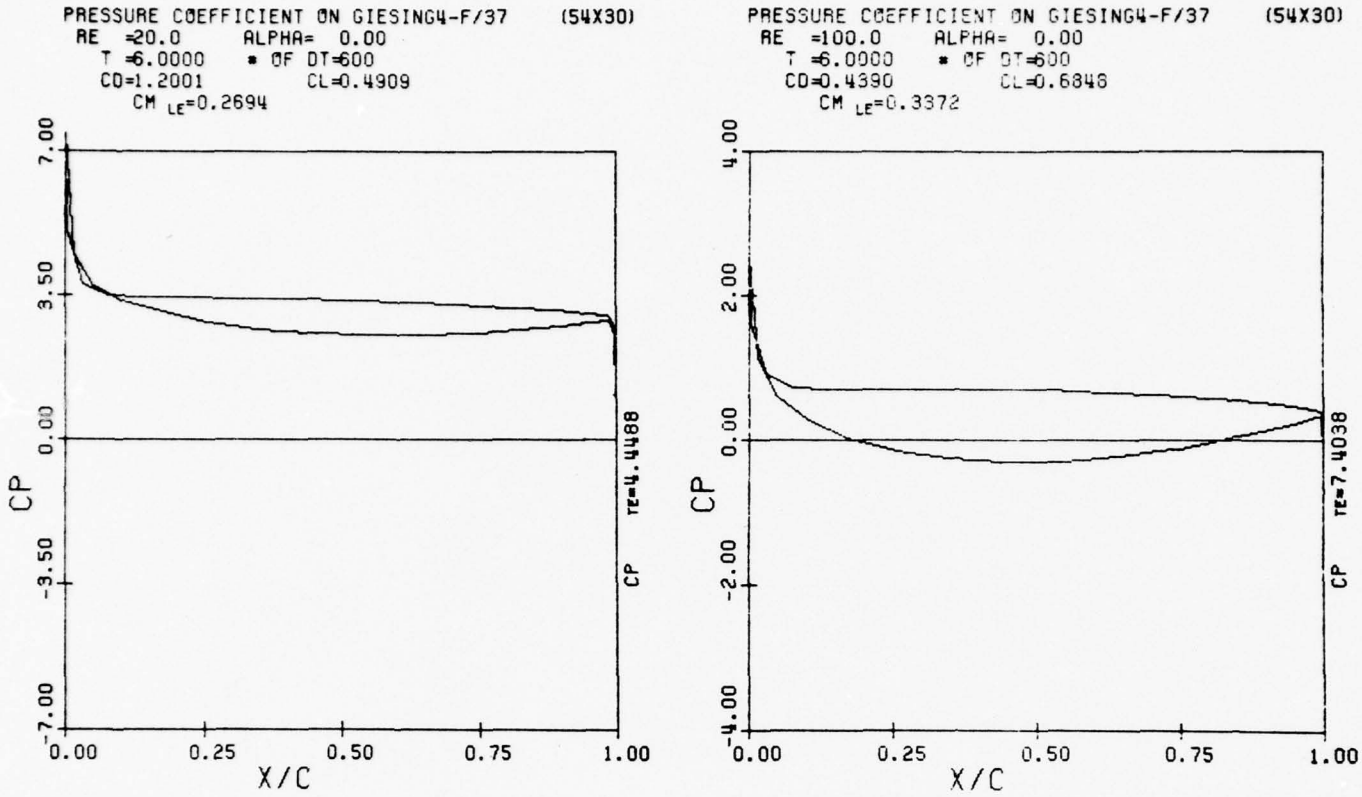

(a) Re = 20

(b) Re = 100

Figure 17. Pressure distribution for two Reynolds numbers, F = 0.5, t = 6.0 - Karman Trefftz Airfoil located 1 chord below a free surface.

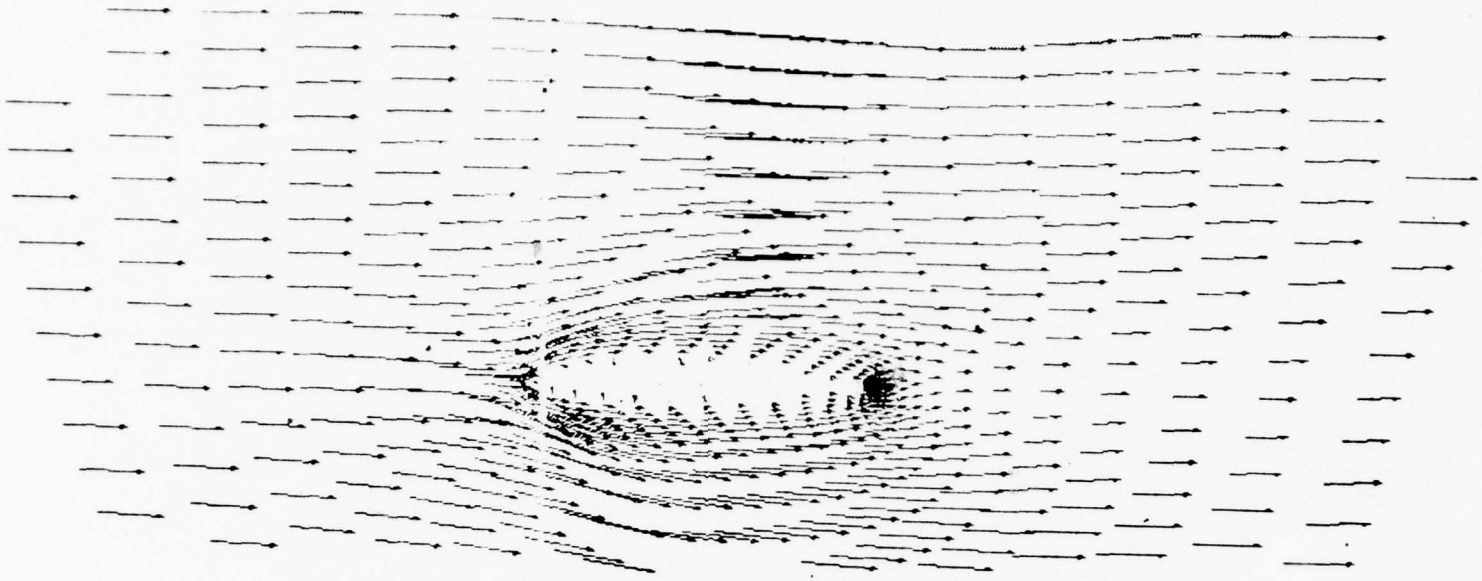

Figure 18. Velocity vector field, Re = 100, F = 0.5, t = 6.0 - Karmon-Trefftz Airfoil located 1 chord below a free-surface.

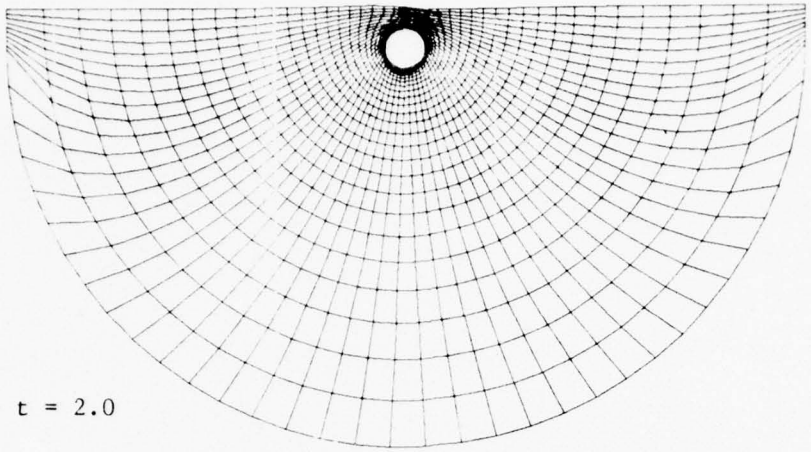

(a) t = 2.0

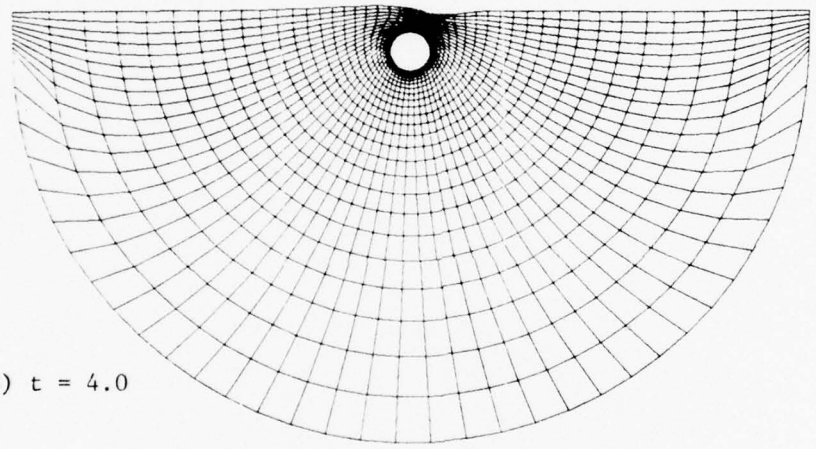

(b) t = 4.0

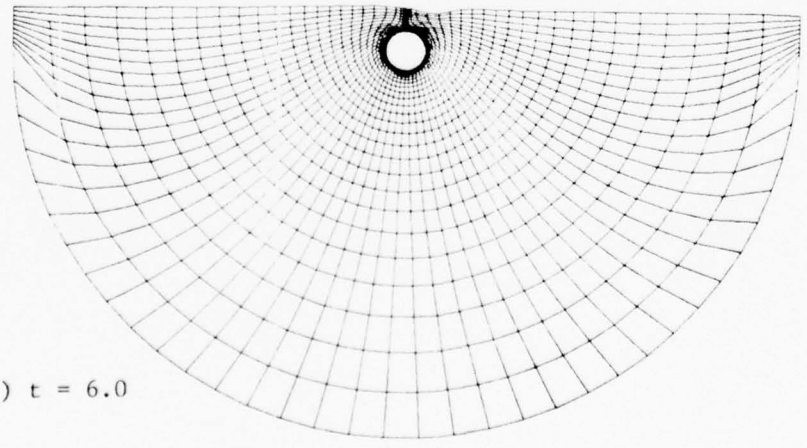

(c) t = 6.0

Figure 19. Coordinate system at three times, Re = 20, F = 0.5 - circular cylinder located 1 chord below free-surface.

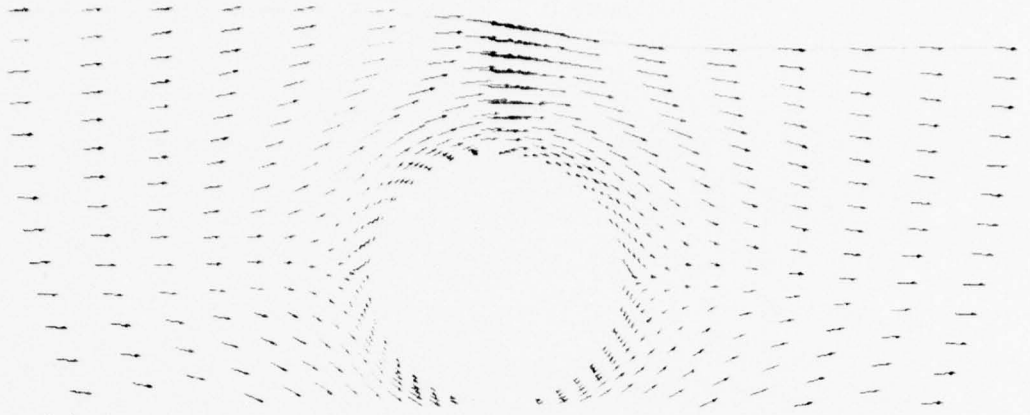

(a) t = 2.0

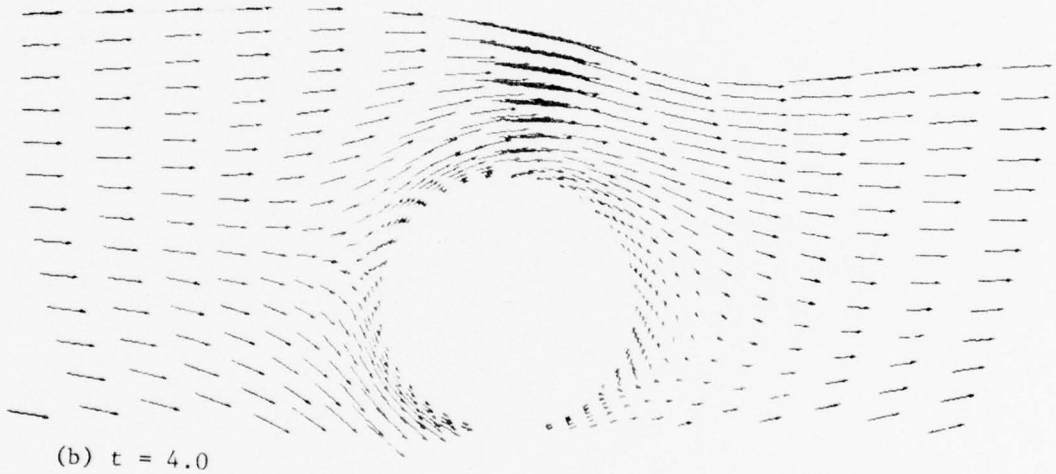

(b) t = 4.0

(c) t = 6.0

Figure 20. Velocity vector field at three times, Re = 20, F = 0.5 - circular cylinder located 1 chord below free-surface.

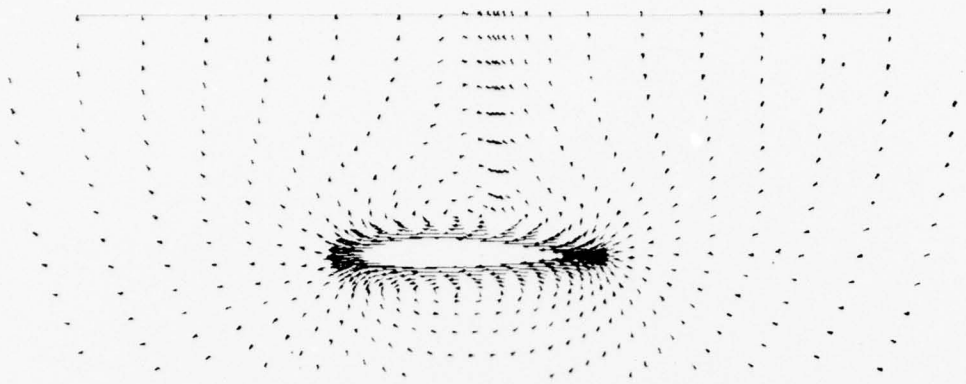

Figure 21. Velocity vector field of Karman-Trefftz Airfoil translating in the negative x-direction, Re = 20, F = 1.0 and t = 0.1 (free stream-fixed coordinates).

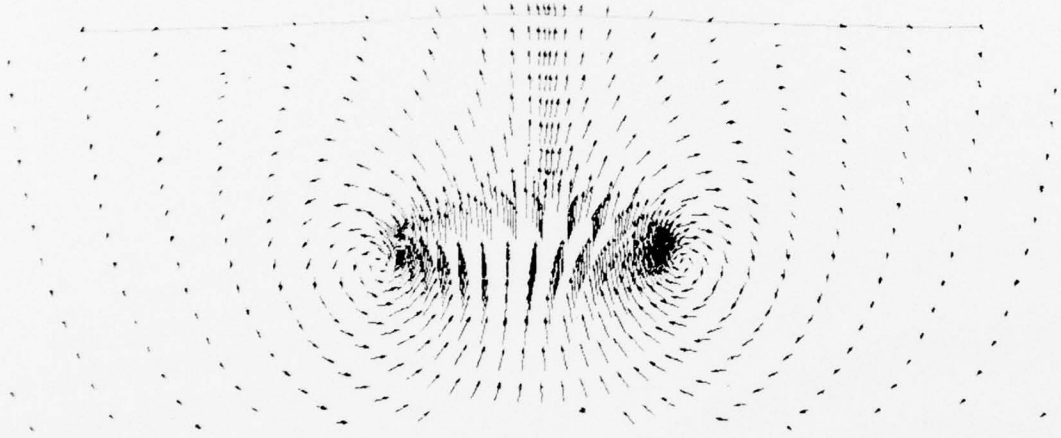

Figure 22. Velocity vector field of Karman-Trefftz Airfoil translating toward free surface, Re = 20, F = 1.0 and t = 1.75 (free stream-fixed coordinates).

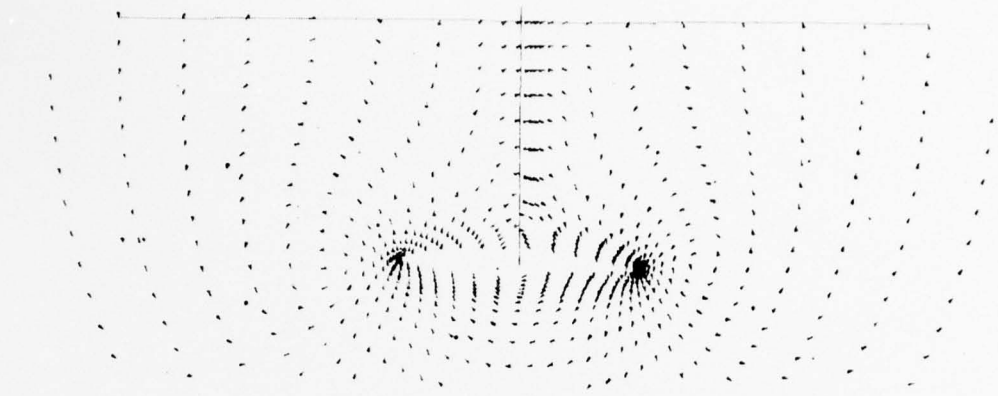

(a) t = 1.0

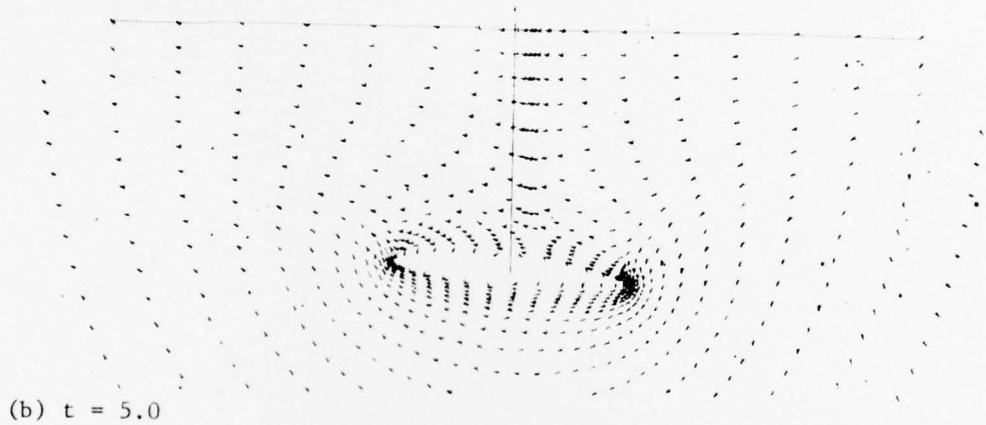

(b) t = 5.0

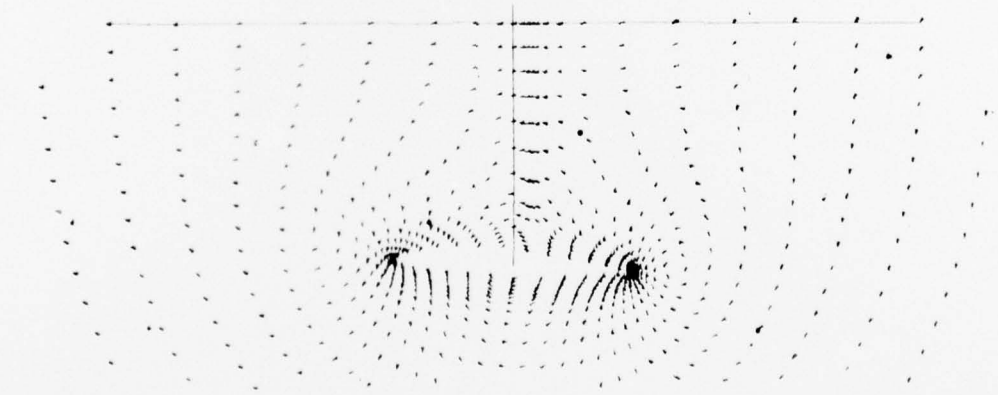

(c) t = 8.0

Figure 23. Velocity vector field of Karman-Trefftz slowly pitching 5° about its center chord at three times, Re = 20, F = 1.0 (free stream-fixed coordinates).

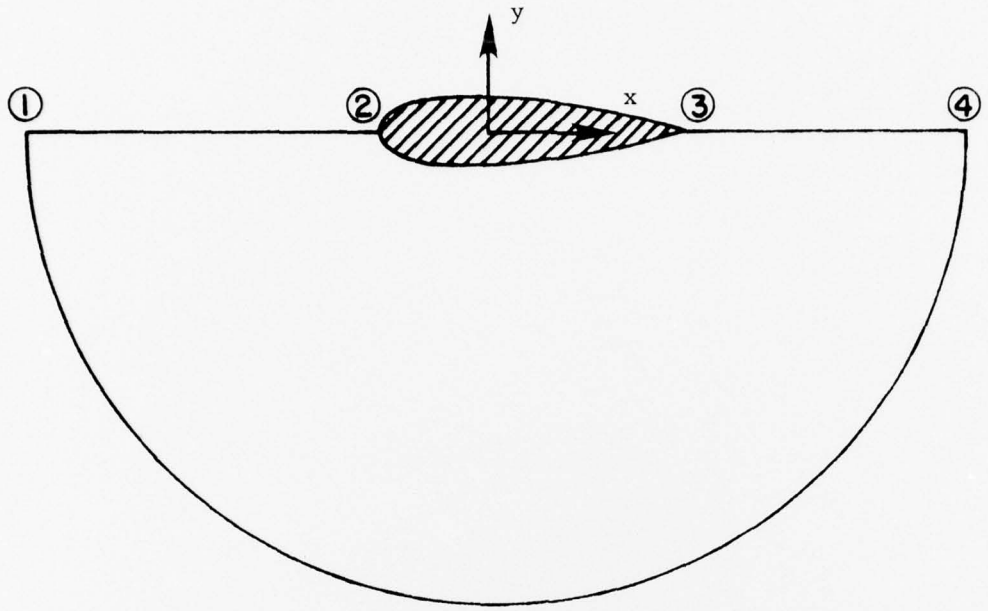

(a) Physical Plane

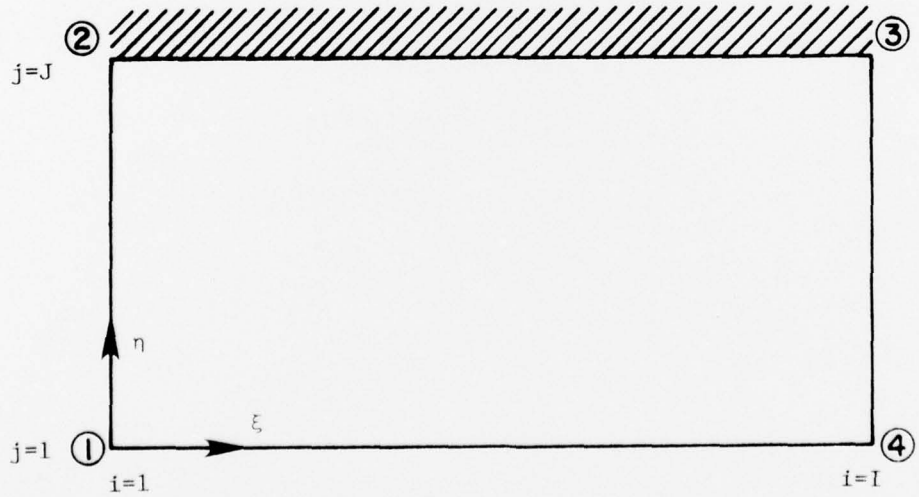

(b) Transformed Plane

Figure 24. Relation Between Physical and Transformed Planes

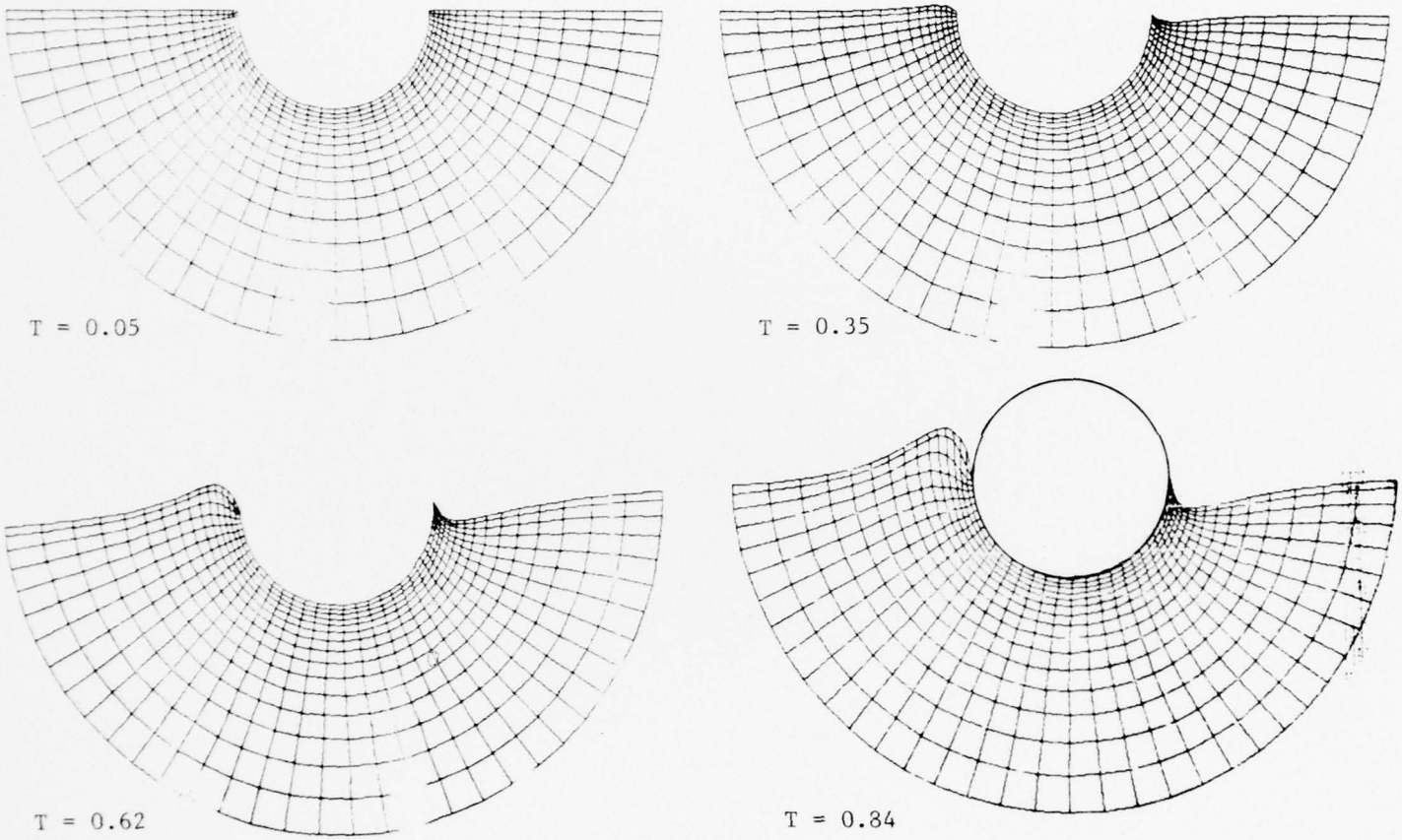

Figure 25. Deforming Coordinate System - Translating Hydrofoil

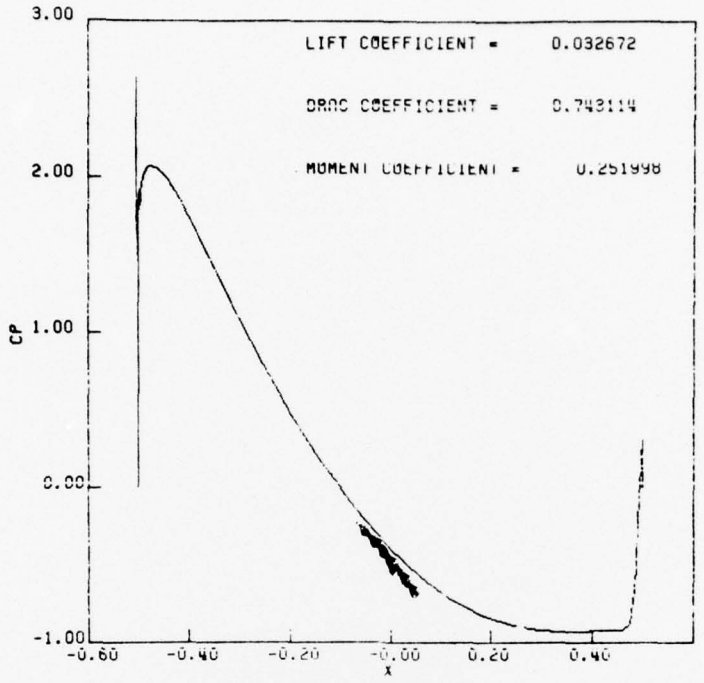

Pressure Distribution

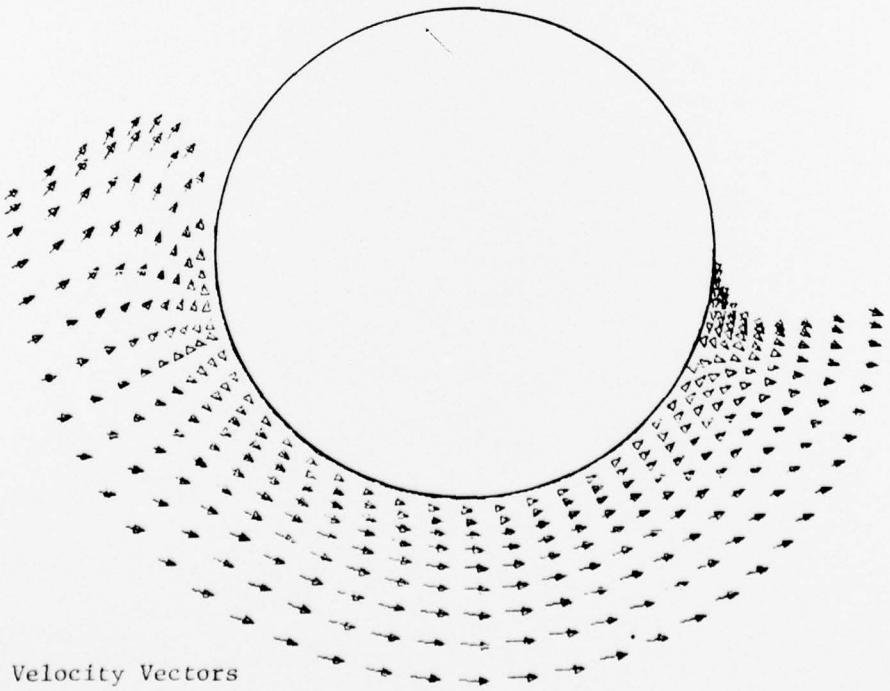

Velocity Vectors

Figure 26. Flow Solution - Translating Hydrofoil. T = 0.84

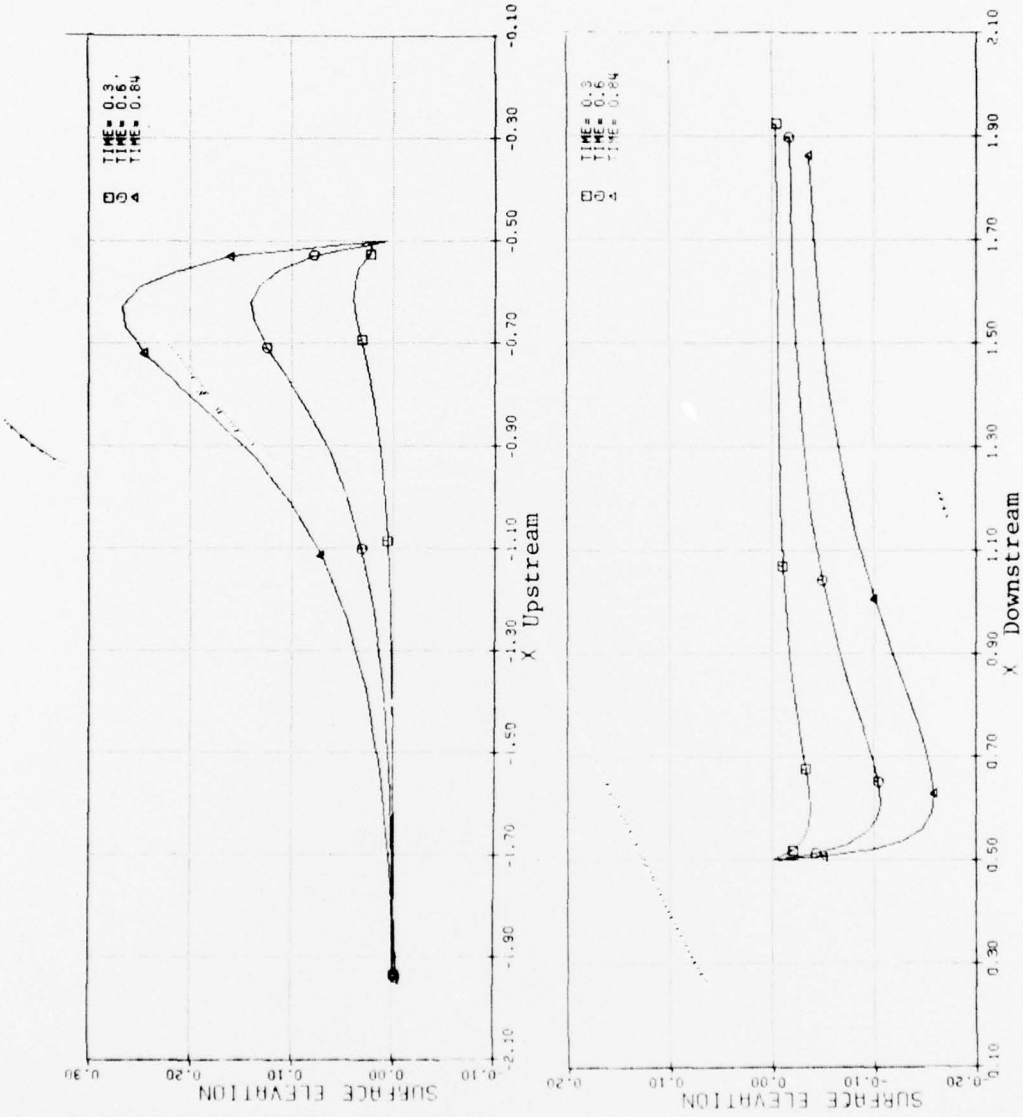

Figure 27. Surface Elevation - Translating Hydrofoil

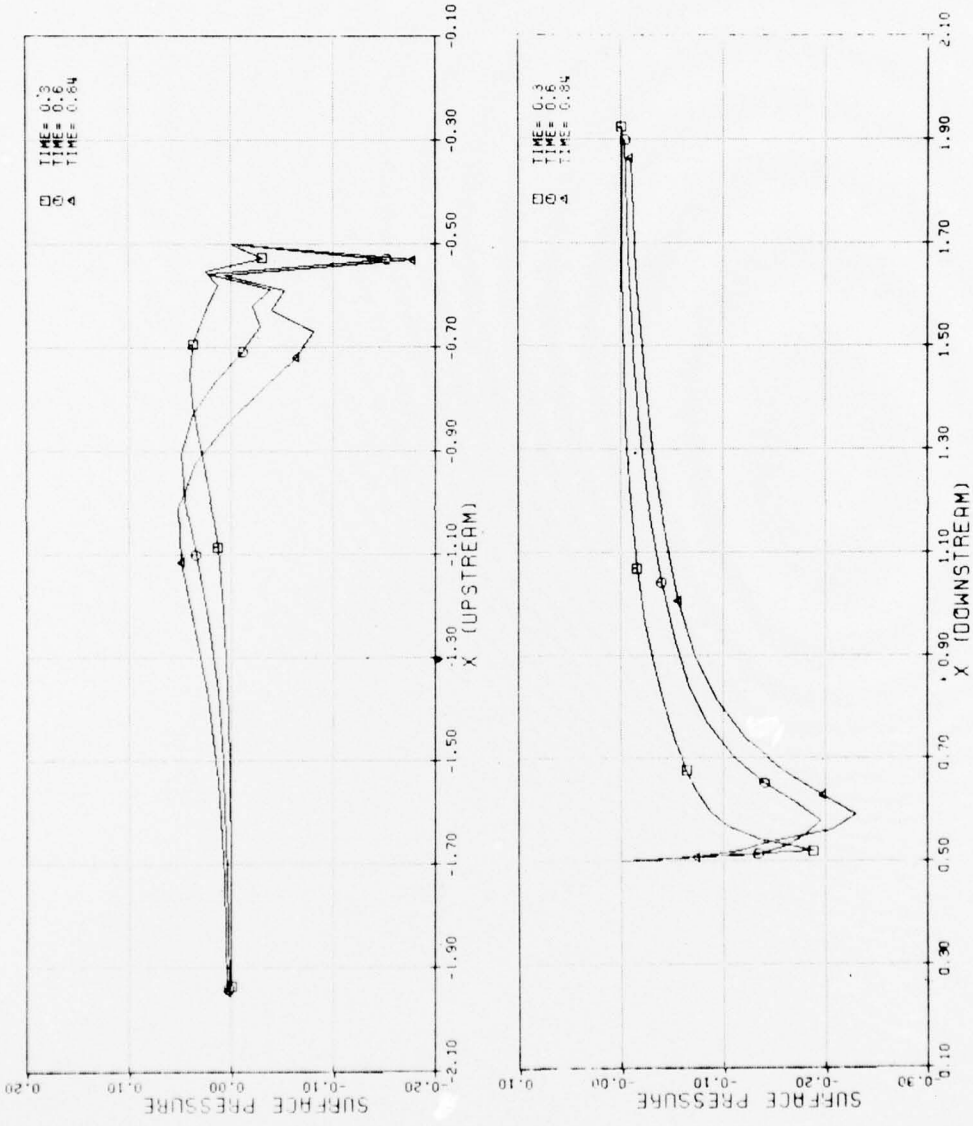

Figure 28. Surface Pressure - Translating Hydrofoil

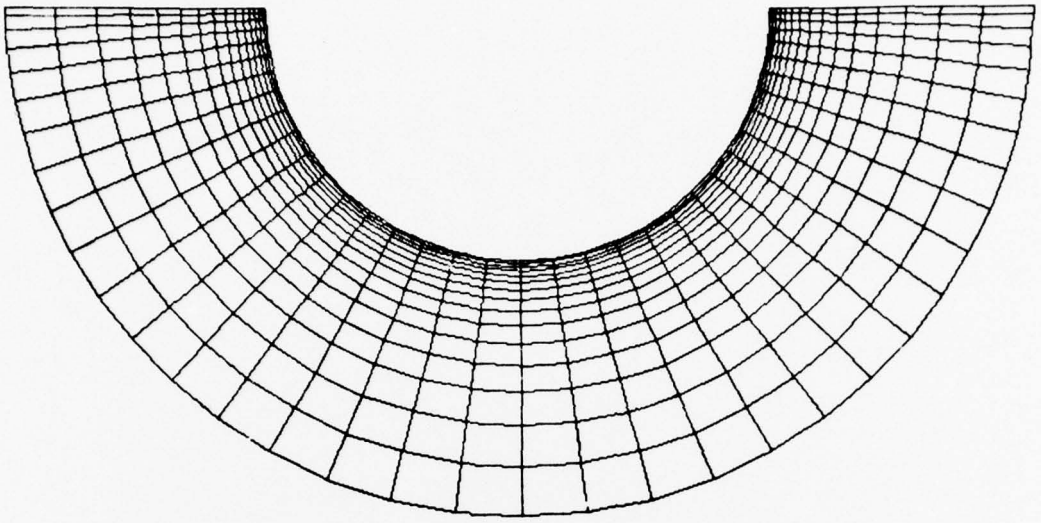

Figure 29. Initial Coordinate System - Plunging Hydrofoil

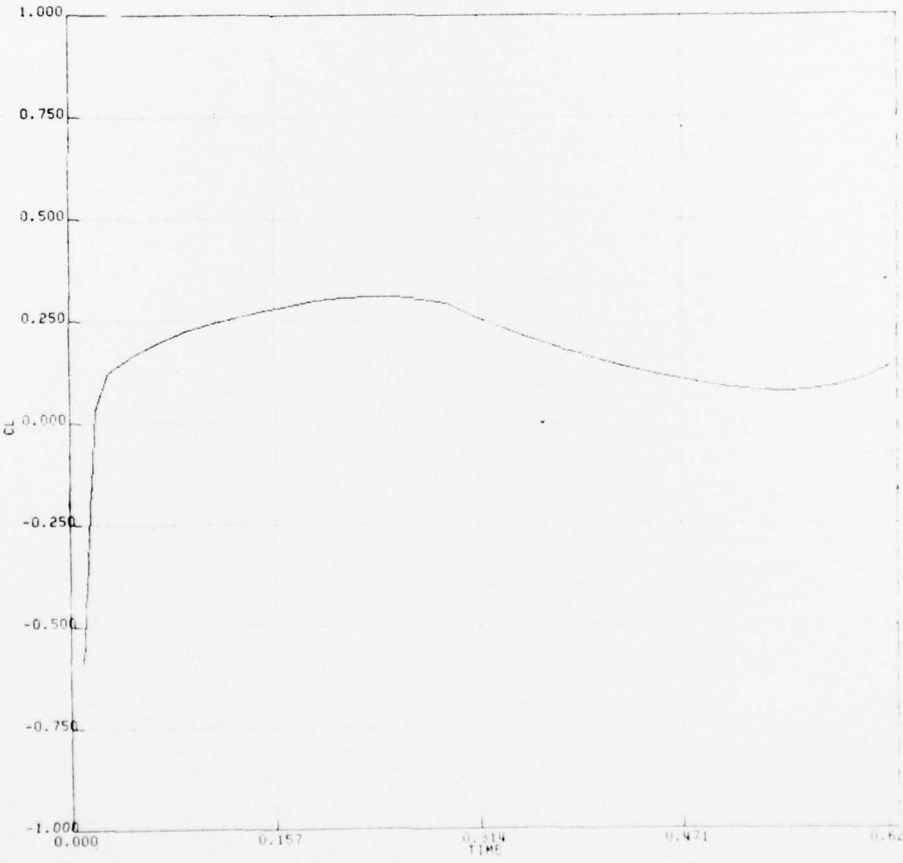

Figure 30. Lift Coefficient - Plunging Hydrofoil

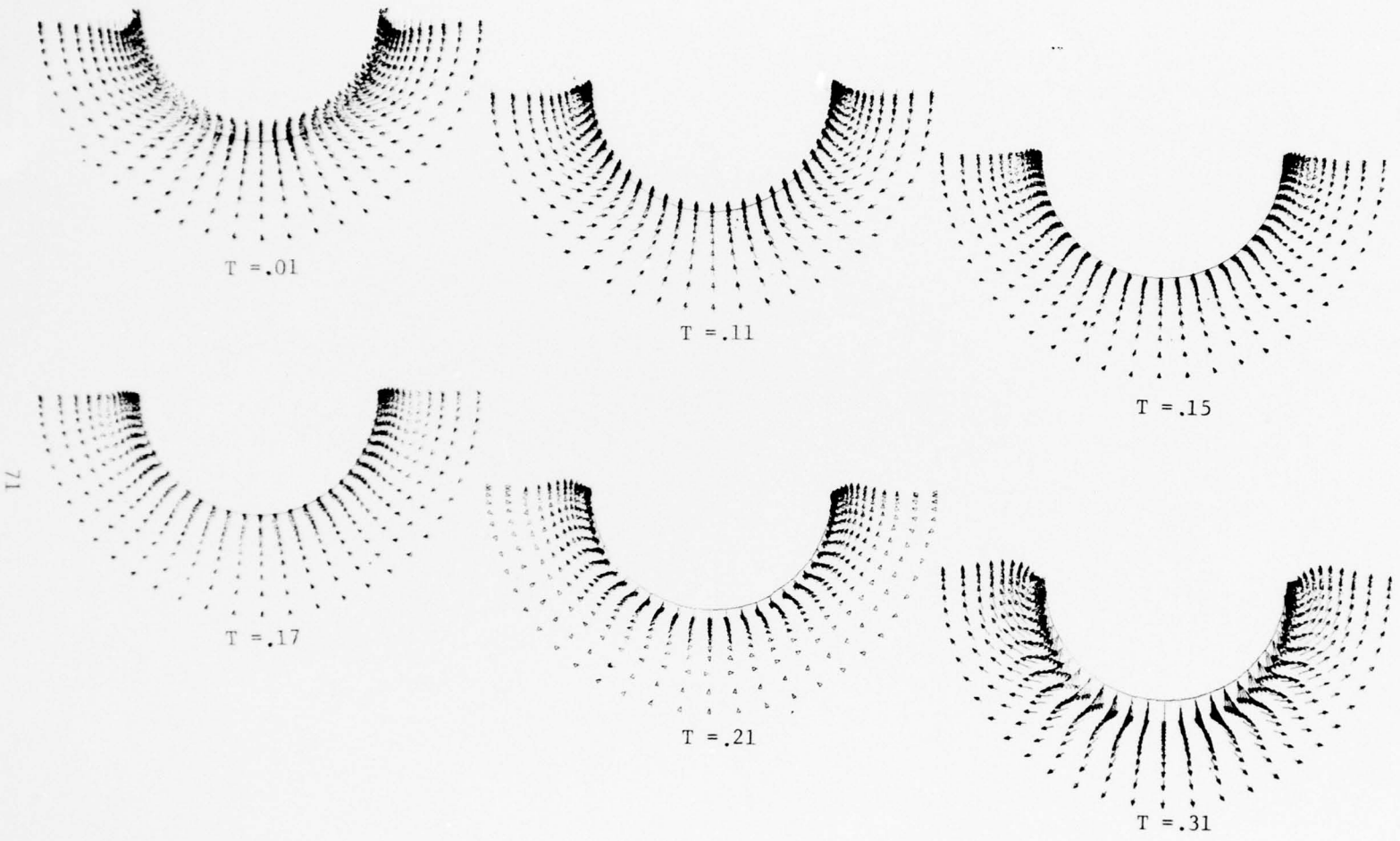

Figure 31. Velocity Vectors - Plunging Hydrofoil (0.001 Amplitude, 0.628 Period)

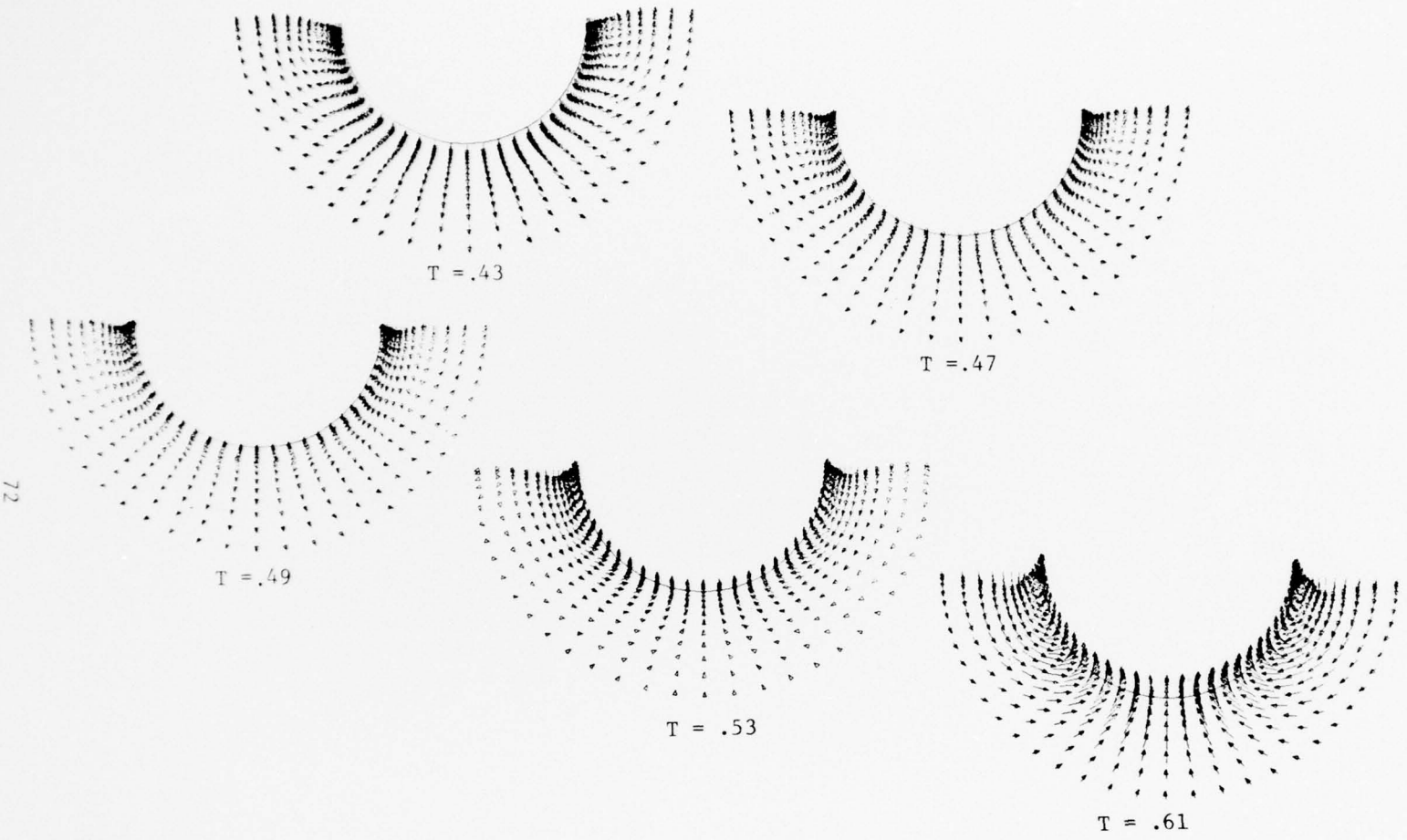

Figure 31. Continued

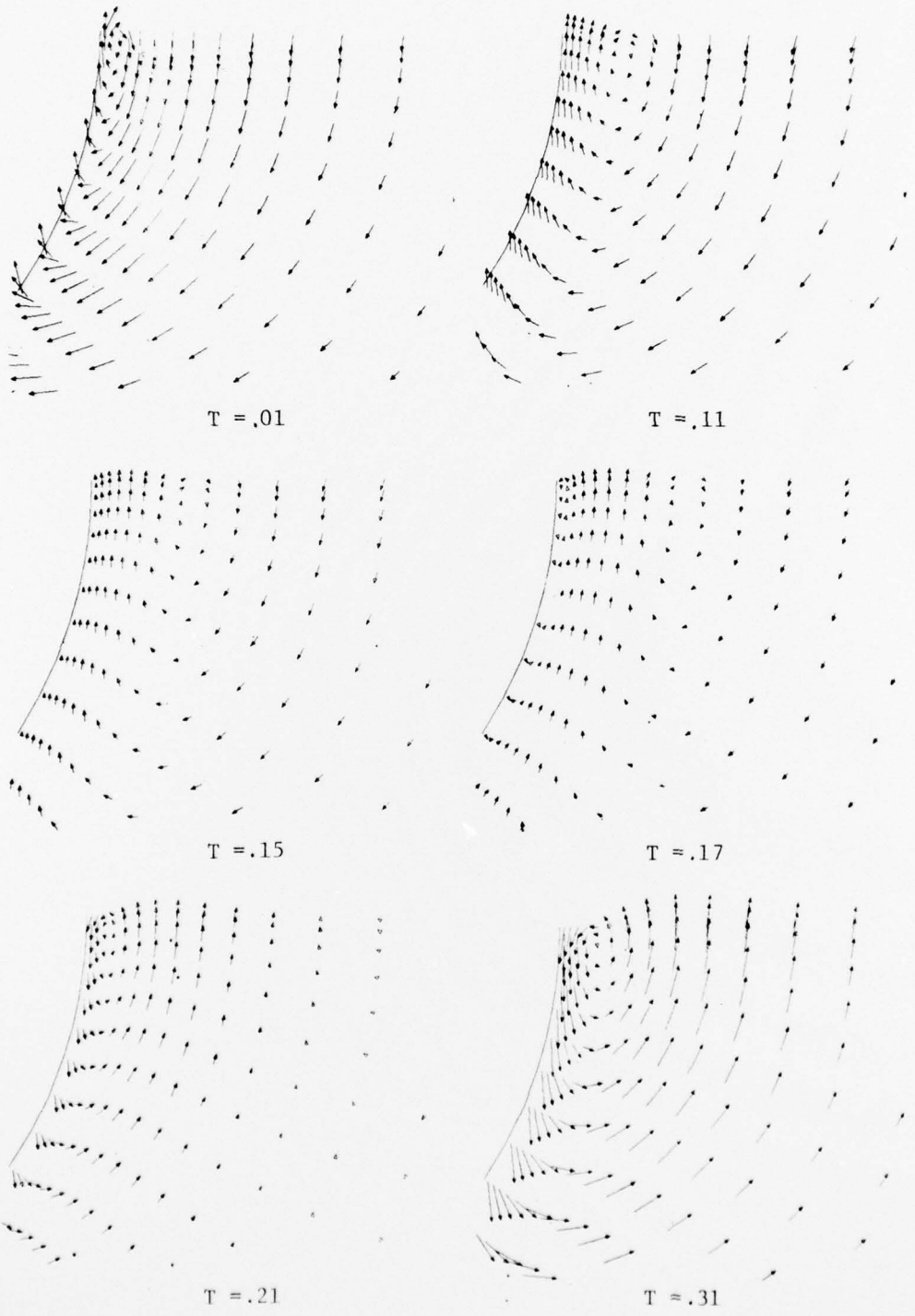

Figure 32. Detail of Surface - Body Contact Region - Plunging Hydrofoil (0.001 Amplitude, 0.628 Period)

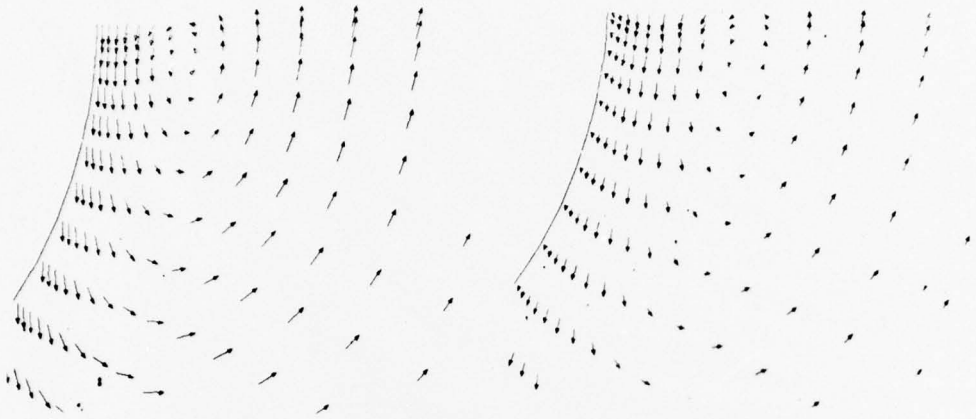

T = .43

T = .47

T = .49

T = .53

T = .61

Figure 32. Continued

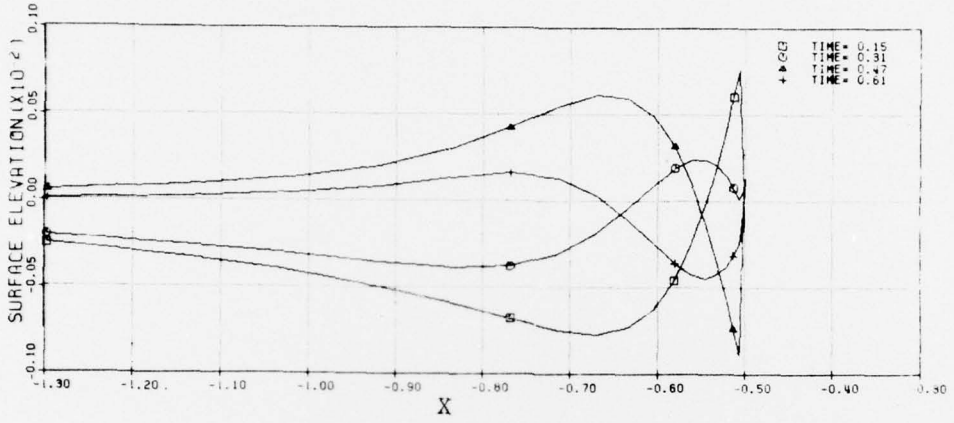

Fig. 33. Surface Elevation - Plunging Hydrofoil (0.001 Amplitude, 0.628 Period)

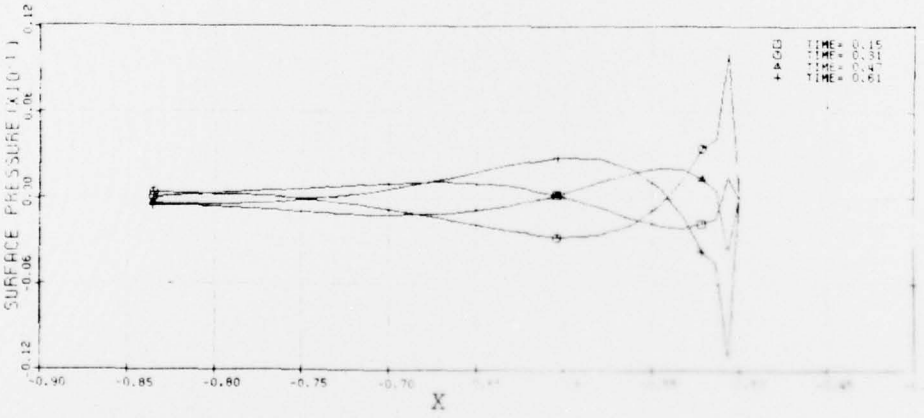

Fig. 34. Surface Pressure - Plunging Hydrofoil (0.001 Amplitude, 0.628 Period)

Unclassified

SECURITY CLASSIFICATION OF THIS PAGE (When Data Entered)

REPORT DOCUMENTATION PAGE		READ INSTRUCTIONS BEFORE COMPLETING FORM
1. REPORT NUMBER MMSU-EIRS-ASE-77-5	2. GOVT ACCESSION NO.	3. RECIPIENT'S CATALOG NUMBER
4. TITLE (and Subtitle) NUMERICAL SOLUTION OF THE NAVIER-STOKES EQUATIONS FOR 2D HYDROFOILS.		5. TYPE OF REPORT & PERIOD COVERED Final Report. 1 Apr 74 — 31 Dec 76 6. PERFORMING ORG. REPORT NUMBER
7. AUTHOR(s) Joe F. Thompson, Samuel P. Shanks, and Ray L. Walker		8. CONTRACT OR GRANT NUMBER(s) N00014-74-C-0373 new
9. PERFORMING ORGANIZATION NAME AND ADDRESS MISSISSIPPI STATE UNIVERSITY Department of Aerophysics & Aerospace Engineering Mississippi State, MS 39762		10. PROGRAM ELEMENT, PROJECT, TASK AREA & WORK UNIT NUMBERS 122301
11. CONTROLLING OFFICE NAME AND ADDRESS Department of the Navy Office of Naval Research Arlington, VA 22217		12. REPORT DATE February 1977 13. NUMBER OF PAGES 60
14. MONITORING AGENCY NAME & ADDRESS (if different from Controlling Office) Office of Naval Research Resident Representative P. O. Box 1274 Huntsville, AL 35807		15. SECURITY CLASS. (of this report) Unclassified 15a. DECLASSIFICATION/DOWNGRADING SCHEDULE N/A

16. DISTRIBUTION STATEMENT (of this Report)

APPROVED FOR PUBLIC RELEASE, DISTRIBUTION UNLIMITED

17. DISTRIBUTION STATEMENT (of the abstract entered in Block 20, if different from Report)

18. SUPPLEMENTARY NOTES

19. KEY WORDS (Continue on reverse side if necessary and identify by block number)

Hydrofoils, Free Surface, Navier-Stokes, Viscous Flow, Computational Fluid Dynamics

20. ABSTRACT (Continue on reverse side if necessary and identify by block number)

This report presents the results of an investigation of the application of numerically-generated boundary-fitted curvilinear coordinate systems in the finite-difference solution of the time-dependent, two-dimensional Navier-Stokes equations for the laminar viscous flow about hydrofoils moving either submerged at a finite depth or in a free surface of a fluid of infinite depth. The hydrofoil may be of arbitrary shape, and its motion may include pitching → next page

DD FORM 1 JAN 73 1473 EDITION OF 1 NOV 65 IS OBSOLETE

390 182

Unclassified

SECURITY CLASSIFICATION OF THIS PAGE (When Data Entered)

2B

(Block 20)

oscillation or oscillation normal or parallel to the plane of the undisturbed free surface as well as translation parallel to this plane. A computer code has been developed that is capable of predicting the flow field, pressure distributions, and force coefficients for this configuration at low Reynolds numbers. The finite-difference solution is implicit in time so that all the difference equations are solved simultaneously by iteration at each time step.